Photosynthetic linear electron flow drives CO2 assimilation in maize leaves

Ginga Shimakawa
Kobe University
Chikahiro Miyake (cmiyake@hawk.kobe-u.ac.jp)
Kobe University https://orcid.org/0000-0002-2426-2377

Article

Keywords: Photosynthesis, Linear electron flow, C4 plants, P700 oxidation, Ferredoxin

Posted Date: February 19th, 2021

DOI: https://doi.org/10.21203/rs.3.rs-222497/v1

***Corresponding Author:** Chikahiro Miyake
Department of Biological and Environmental Science, Faculty of Agriculture, Graduate School of Agricultural Science, Kobe University, 1-1 Rokkodai, Nada, Kobe 657-8501, Japan
Fax: +81-78-803-5851; e-mail: cmiyake@hawk.kobe-u.ac.jp

Title: Photosynthetic linear electron flow drives CO_2 assimilation in maize leaves

Running head: Regulation of photosynthesis in C_4 plants

Author's Addresses: Ginga Shimakawa[1,#] and Chikahiro Miyake[1,2,*]
[1]Department of Biological and Environmental Science, Faculty of Agriculture, Graduate School of Agricultural Science, Kobe University, 1-1 Rokkodai, Nada, Kobe 657-8501, Japan
[2]Core Research for Environmental Science and Technology, Japan Science and Technology Agency, 7 Goban, Chiyoda, Tokyo 102-0076, Japan

Footnotes: [#]Present address: Research Center for Solar Energy Chemistry, Osaka University, 1-3 Machikaneyama, Toyonaka, Osaka 560-8631, Japan

Abstract

Photosynthetic organisms commonly develop the strategy to keep the reaction centre chlorophyll of photosystem I, P700, oxidised for preventing the generation of reactive oxygen species in excess light conditions. In photosynthesis of C_4 plants, CO_2 concentration is kept at higher levels around ribulose 1,5-bisphosphate carboxylase/oxygenase (Rubisco) by the cooperation of the mesophyll and bundle sheath cells, which enables them to assimilate CO_2 at higher rates and to survive under drought stress. However, the regulatory mechanism of photosynthetic electron transport for P700 oxidation is still poorly understood in C_4 plants. Here we assessed gas exchange, chlorophyll fluorescence, electrochromic shift, and near infrared absorbance in the intact leaves of NADP-malic enzyme subtype of C_4 plants maize in a comparison with the C_3 plant field mustard. Instead of the alternative electron sink due to photorespiration, photosynthetic linear electron flow was strongly limited between photosystems I and II dependent on the proton gradient across the thylakoid membrane (ΔpH) in response to the suppression of CO_2 assimilation in maize. The increase of ΔpH for P700 oxidation was caused by the regulation of proton conductance of chloroplast ATP synthase but not by promoting cyclic electron flow, which was supported by linear relationships among CO_2 assimilation rate, linear electron flow, P700 oxidation, ΔpH, and the oxidation rate of ferredoxin. At the scale of intact leaves, the ratio of PSI to PSII was estimated almost 1:1 in both C_3 and C_4 plants. Overall, the photosynthetic electron transport was regulated for P700 oxidation in maize through the same strategies as in C_3 plants only except for the capacity of photorespiration despite the structural and metabolic differences in photosynthesis between C_3 and C_4 plants.

Keyword: Photosynthesis; Linear electron flow; C_4 plants; P700 oxidation; Ferredoxin

Introduction

In chloroplasts of plant leaves, photosynthetic CO_2 assimilation is driven in the Calvin-Benson cycle utilizing NADPH and ATP produced by light energy [1]. In the photosynthetic electron transport system, light energy is absorbed by chlorophyll in photosystems (PS) I and II, producing the photo-oxidised reaction centre chlorophylls, $P700^+$ and $P680^+$, to initiate photosynthetic linear electron flow (LEF) from PSII to PSI *via* the plastoquinone (PQ) pool, the cytochrome (Cyt) b_6/f complex, and plastocyanin (PC). On the electron acceptor side of PSI, $NADP^+$ is reduced to NADPH using electrons from PSI *via* ferredoxin (Fd) and Fd-$NADP^+$ reductase. In PSII, H^+ is released by H_2O oxidation in the luminal side of the thylakoid membrane; in the Cyt b_6/f complex, the Q-cycle pumps stromal H^+ to the luminal side. Both generate a proton gradient (ΔpH) across the thylakoid membrane to produce ATP *via* the chloroplast ATP synthase. In the Calvin-Benson cycle, ribulose 1,5-bisphosphate (RuBP) carboxylase/oxygenase (Rubisco) catalyses the carboxylation of RuBP to produce two molecules of 3-phosphoglycerate (3-PGA), which are then metabolised in the Calvin-Benson cycle with NADPH and ATP. In this process, RuBP is regenerated. On the other hand, Rubisco competitively catalyses the oxygenation of RuBP, when available CO_2 is limited in the presence of sufficient O_2, to produce 3-PGA and 2-phosphoglycolate (2-PG). 2-PG is finally metabolised to 3-PGA in cooperation with the chloroplasts, peroxisomes, and mitochondria using Fd^- and ATP. This is the so-called photorespiration, in which CO_2 is released from glycine in the mitochondria. The production and consumption of both NADPH and ATP are normally balanced to poise the redox state of the photosynthetic electron transport system in C_3 plants [2, 3]. In C_4 plants, the capacity of photorespiration had been degenerated during the evolutionary history [4, 5], instead of the CO_2 concentrating mechanism, where CO_2 is incorporated into phosphoenolpyruvate (PEP) in mesophyll cells and then transported in the form of malate into bundle sheath cells that specifically express Rubisco [6]. Malate is converted to CO_2 and pyruvate around Rubisco by NADP-malic enzyme (ME) with $NADP^+$ as the electron acceptor, and PEP is regenerated in mesophyll cells theoretically with two additional ATP [7, 8]. Because of the structural and metabolic complexities, the regulation of photosynthetic electron transport has been poorly understood in C_4 plants.

Oxidation of P700 is a universal physiological response in photosynthetic organisms to prevent photo-oxidative damage derived from reactive oxygen species (ROS) to PSI by dissipating excess light energy as heat [9] because the inhibition of PSI can be a lethal event for photosynthetic organisms [10]. Actually, P700 is kept oxidised by a variety of molecular mechanisms in response to excess light conditions such as high light and CO_2 limitation [11]. In C_3 plants, P700 oxidation is supported on the donor side by the suppression of electron transport in the Cyt b_6/f complex, dependent on ΔpH

[12, 13]. On the acceptor side, photorespiration replaces CO_2 assimilation, to function as an electron sink for P700 oxidation under limited CO_2 conditions [14]. In C_4 plants, there is little electron sink by photorespiration even at the CO_2 compensation point, different from C_3 plants [5, 15]. It is still not clear how P700 remains oxidised in C_4 plants when CO_2 assimilation is suppressed. One important hypothesis that should be tested is that cyclic electron flow around PSI (CEF) functions to make ΔpH to keep P700 oxidised in C_4 plants. Since CEF is mediated by the electron transport from Fd^- to PQ, theoretically it is capable of pumping H^+ from the stroma to the lumen of the thylakoid membrane in the Q-cycle; this also results in an additional ATP production that is not linked to $NADP^+$ reduction [16]. Especially in C_4 plants, the ratio of PSI to PSII is much higher in isolated bundle sheath cells than in the mesophyll cells, which gives the hypothesis that CEF in bundle sheath cells contributes not only to keeping P700 oxidised but also to meeting the additional ATP demand for C_4 photosynthesis. Unfortunately, there is not currently a method available to directly measure the electron transport rate *via* CEF. The CEF activity has been indirectly estimated mainly from the quantum yield of PSI, which is inevitably under/overestimated dependent on the redox state of PC [2]. Therefore, the extent of CEF activity remains controversial.

In this study, we evaluated gas exchange, chlorophyll fluorescence, electrochromic shift (ECS), and near infrared (NIR) absorbance in the NADP-ME subtype of C_4 plants maize to investigate how photosynthetic electron transport is regulated for P700 oxidation. Although maize did not show the significant capacity of photorespiration, P700 oxidation was tightly coupled with LEF like the C_3 plant field mustard (komatsuna, hereafter mustard), which was supported by the linear relationships among CO_2 assimilation rate, LEF, P700 oxidation, ΔpH, and the Fd^- oxidation rate. The ratio of PSI to PSII was estimated *in vivo* approximately 1:1 in the both C_3 and C_4 plants. These results suggest that maize regulates photosynthetic electron transport for P700 oxidation tightly associated with LEF like C_3 plants but strongly relies it on the ΔpH-dependent suppression of electron transport on the donor side of PSI instead of photorespiratory electron sink on the acceptor side.

Results

Photosynthetic CO_2 assimilation and dark respiration were analysed in both the C_3 plant mustard and the C_4 plant maize simultaneously with chlorophyll fluorescence, ECS, and NIR absorbance. In this study, we analysed *in vivo* photosynthetic parameters at a constant light intensity and different CO_2 partial pressures to simply investigate the effects of limitation of electron sink on the photosynthetic electron transport. Additionally, the C_3 and C_4 intact leaves were measured at atmospheric (21 kPa) and low (1 kPa) O_2, where photorespiration is inhibited. We note that in maize CO_2 is first incorporated into PEP in mesophyll cells, different from C_3 plants, but the decrease of the CO_2 partial pressure in the intercellular space (Ci) finally results in the limitation of the carboxylation reaction of Rubisco in bundle sheath cells.

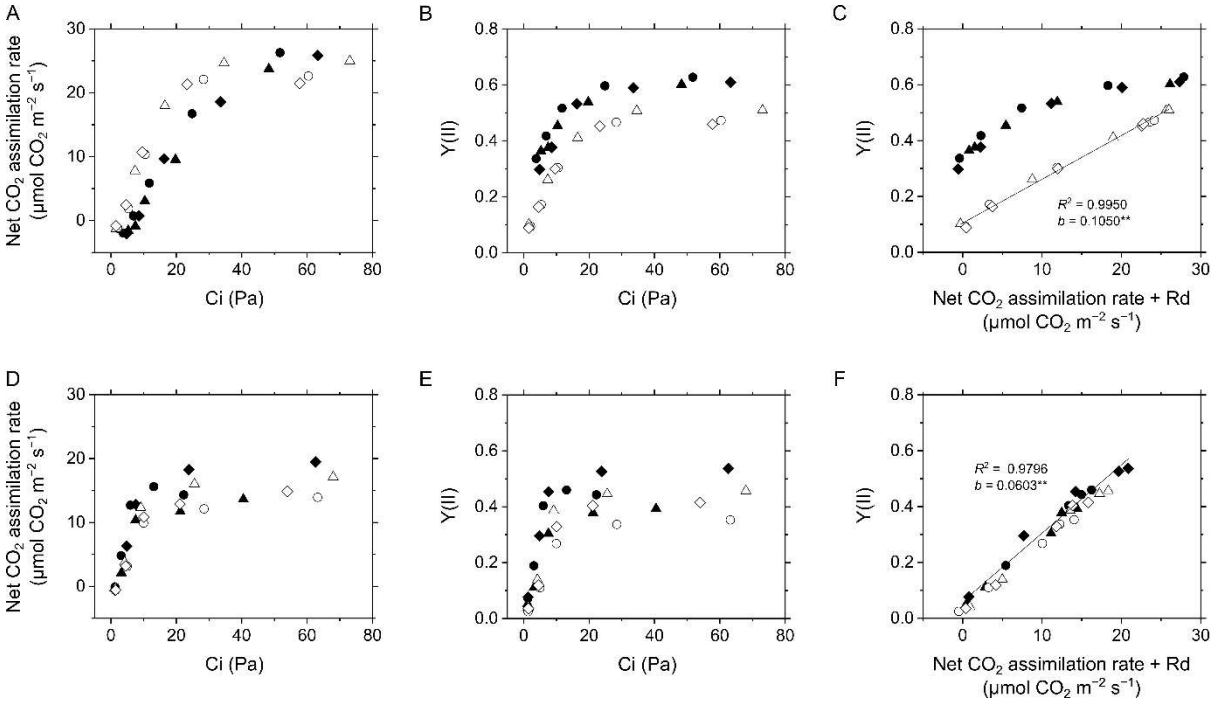

Fig. 1. Photosynthetic CO_2 assimilation and linear electron flow in the C_3 plant mustard (A–C) and the C_4 plant maize (D–F). (A, D) Net CO_2 assimilation rate at various intercellular CO_2 partial pressures (Ci). (B, E) Effective quantum yield of PSII, Y(II), at various Ci. (C, F) Relationship of Y(II) with CO_2 assimilation rate. Dark respiration rate is presented as Rd. Experiments were conducted independently three times as shown in different symbols (biological replicates) at 21 kPa (closed symbols) and 1 kPa O_2 (open symbols). Solid lines represent estimated linear regression of the data at 1 kPa (C) and 21 kPa O_2 (F) (R^2, coefficient of determination). The y-intercepts (b) were tested based on the null hypothesis: $^{**}p<0.005$.

In mustard, the net CO_2 assimilation rate was higher at 1 kPa than at 21 kPa O_2 when CO_2 assimilation was limited by Ci (Fig. 1A), whereas the effective quantum yield of PSII, Y(II), was kept high uncoupled from CO_2 assimilation (Fig. 1B and C). However, maize did not show any difference in net CO_2 assimilation and Y(II) between different O_2 partial pressures (Fig. 1D and E), which is in accordance with a small contribution, if any, of photorespiration to the capacity of electron sink. As a result, Y(II) has a linear relationship with the sum of net CO_2 assimilation rate and dark respiration rate (Rd) in maize (Fig. 1F). These typical photosynthetic characteristics of C_3 and C_4 plants have already

been established in previous studies, and extra Y(II) in mustard is known to be due almost exclusively to photorespiration [5, 15, 17, 18, 19, 20]. In the other word, Y(II) reflects LEF mainly derived from CO_2 assimilation and photorespiration in angiosperms [13, 21, 22]. The inferred reduction level of the PQ pool (1 – qL) and non-photochemical quenching (NPQ) were also calculated from chlorophyll fluorescence in mustard and maize, both of which increased at low Ci (Supplemental Fig. S1). In mustard, limiting photorespiration at 1 kPa O_2 caused the further increase of 1 – qL at low Ci, whereas NPQ slightly decreased in this condition (Supplemental Fig. S1A and B).

Next, we evaluated the oxidation of P700 in the relationship with LEF reflected in Y(II) (Fig. 2). In mustard at 21 kPa O_2, the oxidation level of P700 increased monotonously with the decrease in Y(II) (Fig. 2A) although the PQ pool was suggested to be reduced at low Ci (Supplemental Fig. S1B). That is, photosynthetic electron transport is limited between PSII and PSI, presumably at the Cyt b_6/f complex. However, at 1 kPa O_2, P700 started to be kept reduced when Y(II) < 0.3 (Fig. 2A), which suggests that the electron sink by photorespiration is required for P700 oxidation [14]. Unlike mustard, P700 continued to remain oxidised in maize even at 1 kPa O_2 except under an extreme CO_2 limitation (< 1.5 Pa)(Fig. 2B). The inverse proportional relationship in the redox states of the PQ pool and P700 suggested that LEF was limited by the suppression of electron transport at the Cyt b_6/f complex in maize as in C_3 plants (Fig. 2 and Supplemental Fig. S1).

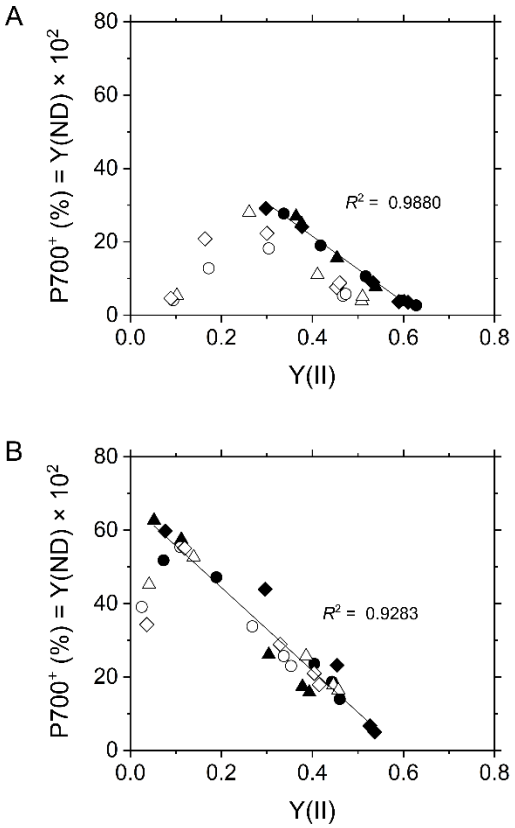

Fig. 2. Relationship of P700 oxidation with effective quantum yield of PSII, Y(II), at various intercellular CO_2 partial pressures in the C_3 plant mustard (A) and the C_4 plant maize (B). Experiments were conducted independently three times as shown in different symbols (biological replicates) at 21 kPa (closed symbols) and 1 kPa O_2 (open symbols). Solid lines represent estimated linear regression of the data at 21 kPa O_2 (R^2, coefficient of determination).

To investigate molecular mechanisms for P700 oxidation in response to the limitation of electron sink, we evaluated the thylakoid membrane potential by ECS analysis in the transition from

light to dark at the steady-state photosynthesis (Fig. 3). We note that the ECS parameters are dependent on the properties of the leaves, not only the density of chloroplasts, but also the content of light-harvesting complexes that house the shifted pigments. Therefore, it is difficult to make any quantitative conclusions for the differences in the amplitudes of ECS parameters between mustard and maize. In the so-called dark-interval relaxation kinetics, *proton motive force* (*pmf*) in the light is defined as the total rapid (< 1 s) change in the ECS signal upon rapidly switching off the light, which increased with the limitation of CO_2 in both mustard and maize at 21 kPa O_2 (Fig. 4A and D). However, in mustard *pmf* was not enhanced in response to the suppression of CO_2 assimilation at 1 kPa O_2,

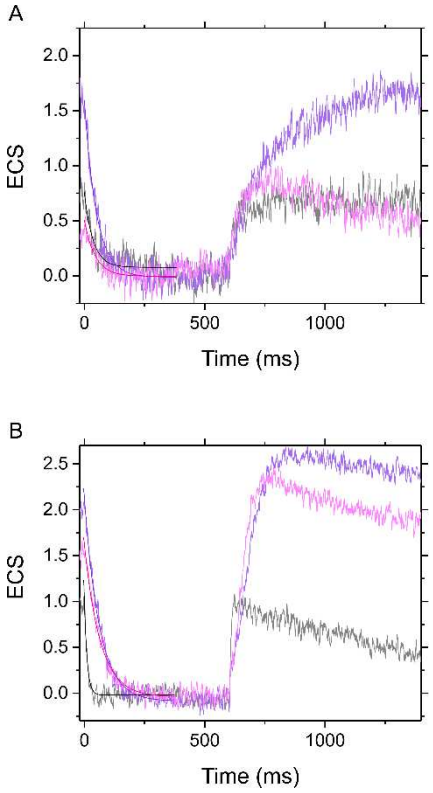

Fig. 3. Dark-interval relaxation kinetics of electrochromic shift (ECS) in the C_3 plant mustard (A) and the C_4 plant maize (B) under ambient air (40 Pa CO_2, 21 kPa O_2; black), low CO_2 (1 Pa CO_2, 21 kPa O_2; purple), and low CO_2/O_2 (1 Pa CO_2, 1 kPa O_2; pink). Red actinic light (550 µmol photons m^{-2} s^{-1}) was turned off at 0 ms for 600 ms during the steady-state photosynthesis. The kinetics were fit to mono exponential decay (R^2, coefficient of determination: 0.7017, 0.9454, and 0.6868 in A; 0.8814, 9868, and 0.9801 in B respectively).

where photorespiration is inhibited (Fig. 4A). That is, photorespiration functions as the electron sink to sustain LEF, supporting the increase of *pmf* in C_3 plants [14]. Nevertheless, we found the increase of *pmf* independent of photorespiration in maize (Fig. 4D). Proton conductance of the ATP synthase (g_{H^+}) is calculated as the rate constant of the mono-exponential ECS decay [23], which increased with Ci and were then saturated as in the trend of CO_2 assimilation rate regardless of O_2 partial pressures in both mustard and maize (Fig. 4B and E). Further, the initial decay rate of the ECS changes is termed as relative light-driven proton flux through the chloroplast ATP synthase, the so-called v_{H^+} [24], which is correlated with the sum of net CO_2 assimilation rate and Rd at 1 kPa O_2 in mustard (Fig. 4C). In mustard at 21 kPa O_2, a part of v_{H^+} was uncoupled from the CO_2 assimilation rate (Fig. 4C), like the case of Y(II) (Fig. 1C), which suggested that v_{H^+} has almost the linear relationship with LEF derived from CO_2 assimilation and photorespiration in C_3 intact leaves. In the case of maize leaves, the relationship of v_{H^+} with photosynthetic CO_2 assimilation does not seem to be linear, different from that of Y(II), at

both 21 and 2 kPa O_2 (Fig. 4F). We note that v_H^+ decreased with photosynthetic CO_2 assimilation larger in lower Ci conditions (Fig. 4F), implying that ATP is utilized in a different manner at different Ci levels.

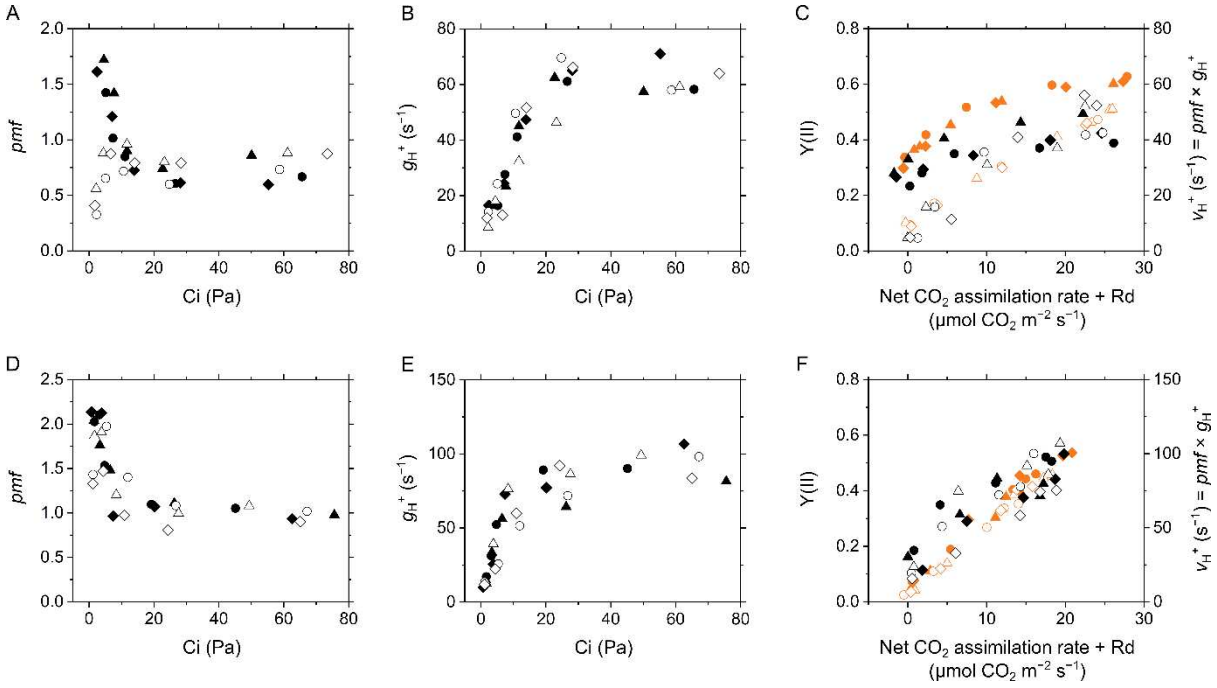

Fig. 4. Electrochromic shift (ECS) parameters in the C_3 plant mustard (A–C) and the C_4 plant maize (D–F). (A, D) *Proton motive force* (*pmf*) at various intercellular CO_2 partial pressures (Ci). (B, E) Proton conductance of the chloroplast ATP synthase (g_H^+) at various Ci. (C, F) Relationship of proton efflux rate *via* the ATP synthase (v_H^+) with CO_2 assimilation rate. Effective quantum yield of PSII, Y(II), are also shown in orange symbols. Dark respiration rate is presented as Rd. Experiments were conducted independently three times as shown in different symbols (biological replicates) at 21 kPa (closed symbols) and 1 kPa O_2 (open symbols).

Theoretically, *pmf* includes two components: ΔpH and transmembrane difference in the electric field (ΔΨ), which can be distinguished by the post-illumination transient change in ECS, and the former component triggers the suppression of electron transport in the Cyt b_6/f complex [25]. Like P700 oxidation, ΔpH showed the linear relationship with LEF at 21 kPa O_2 in both mustard and maize. The formation of ΔpH was disturbed at 1 kPa O_2 in mustard and also in maize at very low Ci (Fig. 5A and C). The increase of ΔpH was associated with NPQ (Supplemental Fig. S1B), which was in agreement with that NPQ at PSII is stimulated by ΔpH [26]. There were two possibilities assumed for the lumen acidification: (1) H^+-pumping from stroma into the thylakoid lumen was promoted; or (2) H^+-leakage from the lumen to stroma was blocked. Both mustard and maize showed the linear relationship of g_H^+ with LEF reflected in Y(II) (Fig. 5B and D), which suggested that limiting g_H^+ leads to the increase in ΔpH, resulting in P700 oxidation.

In this study, we investigated the redox state of Fd at the steady state of photosynthesis in both mustard and maize using a Klas-NIR spectrophotometer. The maximum amplitude of photo-reducible Fd was determined by the standard method in advance as shown in Supplemental Fig. S2. The decay of Fd^- in the transition from light to dark was mono-exponentially fit, giving the amplitude and the oxidation rate of Fd^- (Fig. 6). Exceptionally, a biphasic decay manner was recognised in the kinetics at 1 Pa CO_2 and 1 kPa O_2 in maize (Supplemental Fig. S3). The slow component remains to be

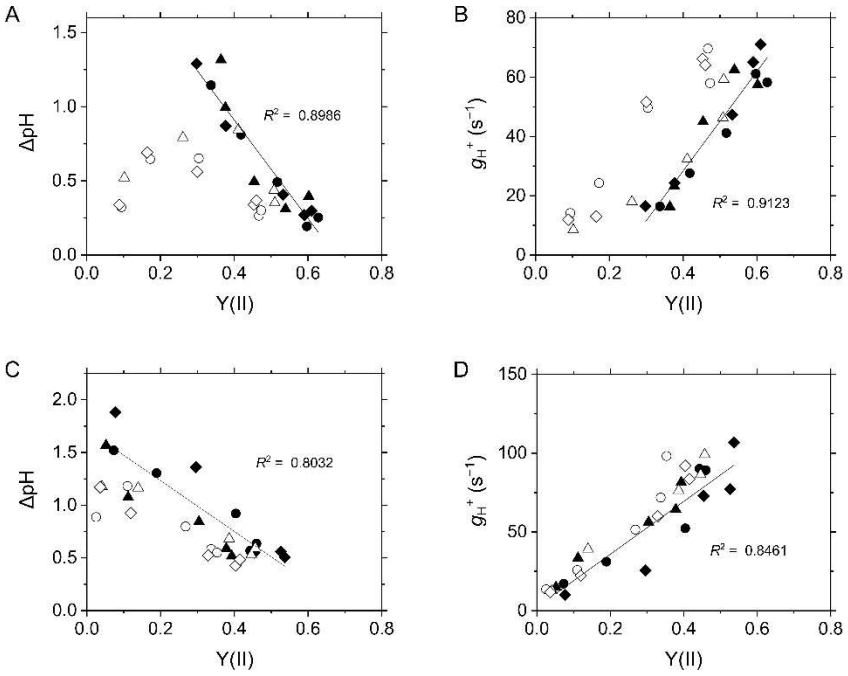

Fig. 5. Relationships of the proton gradient across the thylakoid membrane (ΔpH; A, C) and the proton conductance of the chloroplast ATP synthase (g_H^+; B, D) with effective quantum yield of PSII, Y(II), at various intercellular CO_2 partial pressures in the C_3 plant mustard (A, B) and the C_4 plant maize (C, D). We note that ΔpH and g_H^+ were separately measured from Y(II) at the same ambient CO_2 partial pressures. Experiments were conducted independently three times as shown in different symbols (biological replicates) at 21 kPa (closed symbols) and 1 kPa O_2 (open symbols). Solid lines represent estimated linear regression of the data at 21 kPa O_2 (R^2, coefficient of determination).

identified, but it was clearly negligible compared to LEF because the estimated half time was more than minutes. In mustard, Fd was strongly reduced under CO_2 limitation at 1 kPa O_2, whereas it was totally kept oxidised at 21 kPa O_2 (Fig. 6A and 7A), indicating that photorespiration functions as the electron sink to relieve the acceptor-side limitation of PSI. In maize, Fd^- was gradually accumulated with the decrease in Ci regardless of O_2 (Fig. 6B and 7B). The intact leaves of mustard showed a linear relationship of Fd^- oxidation rate with Y(II) and its *y*-intercept was close to zero (Fig. 7C), which is in agreement with the recent study on C_3 plants [27]. Further, the same trend was observed also in maize leaves (Fig. 7D). That is, LEF estimated from Y(II) clearly corresponds to the electron transport *via* Fd in the situations where ΔpH increased and P700 was oxidised in response to the limitation of electron sink in both mustard and maize.

We also plotted effective quantum yield of PSI, Y(I), against Y(II), which is a conventional method to evaluate CEF activity used in numerous previous and recent reports. In mustard at 21 kPa O_2, we observed a linear relationship between Y(I) and Y(II) with extra Y(I) to Y(II) at lower Ci (Fig. 8A). Additionally, Y(I) showed no linear relationship with Y(II) in mustard at 1 kPa O_2 and maize at both 21 and 1 kPa O_2, resulting in the extra Y(I) (Fig. 8A and C), different from the relationship of Fd^- oxidation rate with Y(II). Here, we also evaluated the oxidation of PC and plotted it against Y(II). In mustard, PC was kept more oxidized at lower Ci, but it was reduced where photorespiration was inhibited (Fig. 8B), like P700 (Fig. 2A). In maize PC was reduced with the decrease in Y(II) less than 0.2, although it was

194 more oxidized at lower Ci if Y(II) was >0.2, finally giving a curved plot (Fig. 8D). Interestingly, the extra

195 Y(I) to Y(II) was coincided with the oxidation of PC (Fig. 8).

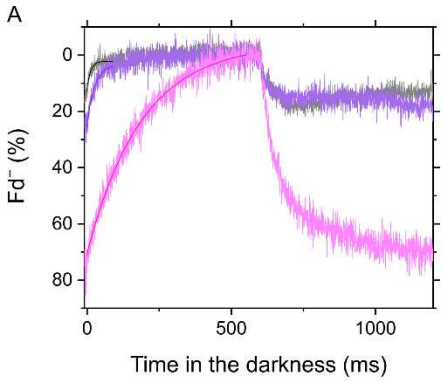

Fig. 6. Dark-interval relaxation kinetics of ferredoxin (Fd^-) in the C_3 plant mustard (A) and the C_4 plant maize (B) under ambient air (40 Pa CO_2, 21 kPa O_2; black), low CO_2 (1 Pa CO_2, 21 kPa O_2; purple), and low CO_2/O_2 (1 Pa CO_2, 1 kPa O_2; pink). Red actinic light (550 µmol photons $m^{-2} s^{-1}$) was turned off at 0 ms for 600 ms during the steady-state photosynthesis. The kinetics were fit to mono exponential decay (R^2, coefficient of determination: 0.6628, 0.8816, and 0.9788 in A; 0.6612 and 0.8307 in B). Only Fd^- kinetics in maize under low CO_2/O_2 was fit to biphasic exponential decay (R^2: 0.9405).

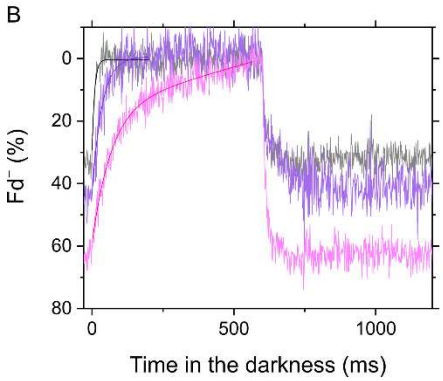

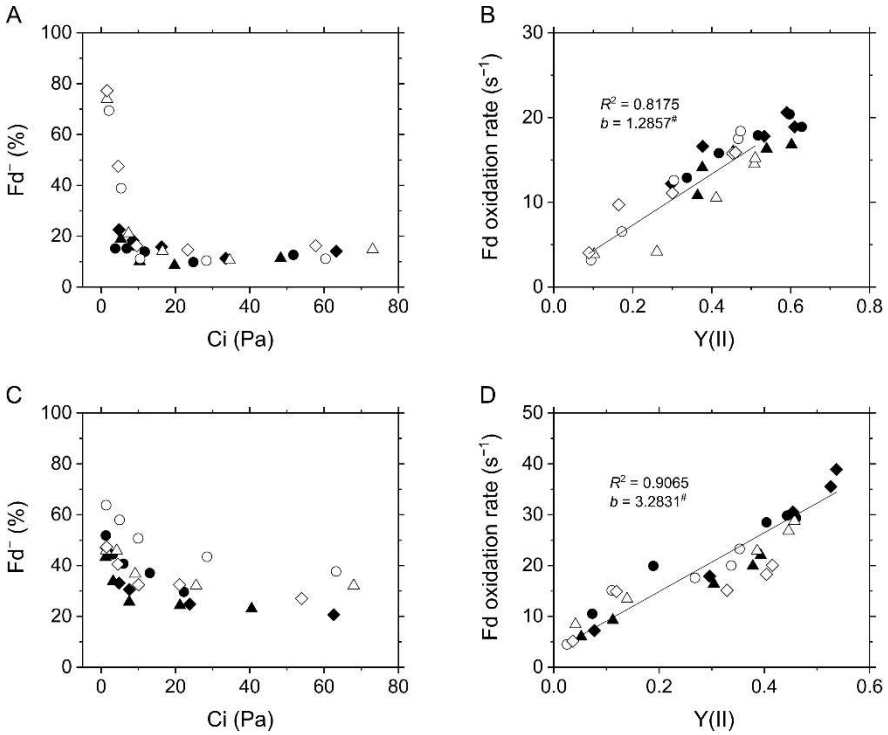

Fig. 7. *In vivo* measurement for the redox state of ferredoxin (Fd) in the C_3 plant mustard (A, B) and the C_4 plant maize (C, D). (A, C) The Fd reduction during the steady-state photosynthesis at various intercellular CO_2 partial pressures (Ci). (B, D) Relationship of Fd^- oxidation rate with effective quantum yield of PSII, Y(II), at various Ci. Experiments were conducted independently three times as shown in different symbols (biological replicates) at 21 kPa (closed symbols) and 1 kPa O_2 (open symbols). Solid lines represent the estimated linear regressions of the data at 1 kPa (B) and 21 kPa O_2 (D), respectively (R^2, coefficient of determination). The *y*-intercepts (*b*) were tested based on the null hypothesis: $^{\#}p>0.05$.

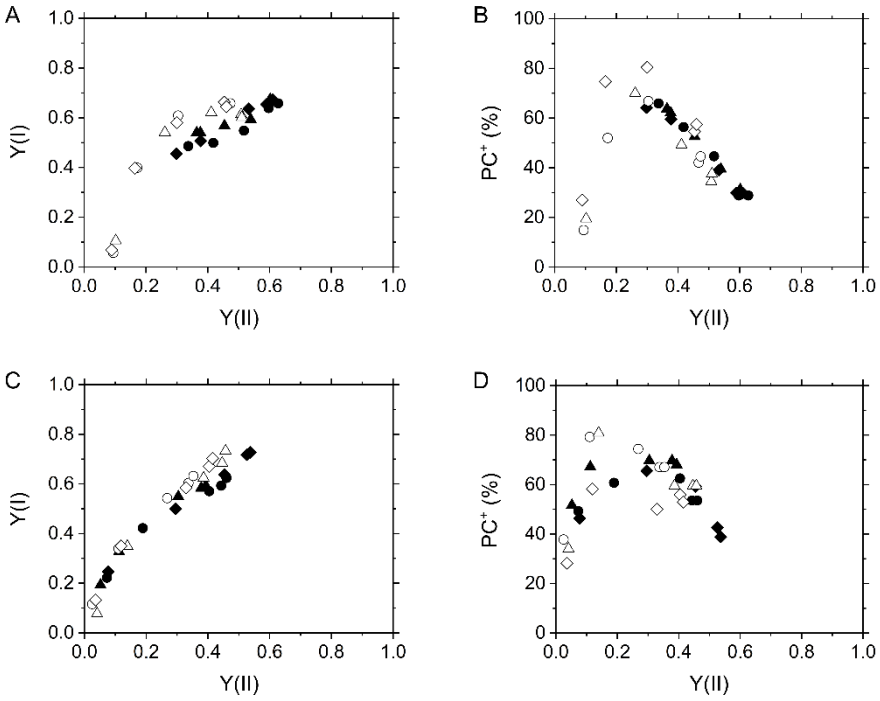

Fig. 8. Relationships of effective quantum yield of PSI, Y(I) (A, C), and plastocyanin (PC) oxidation (B, D) with effective quantum yield of PSII, Y(II), at various intercellular CO_2 partial pressures in the C_3 plant mustard (A, B) and the C_4 plant maize (C, D). Experiments were conducted independently three times as shown in different symbols (biological replicates) at 21 kPa (closed symbols) and 1 kPa O_2 (open symbols).

The linear relationships among CO_2 assimilation rate, Y(II), P700 oxidation, ΔpH, and Fd^- oxidation rate (Fig. 1, 2, 5, and 7) suggested that the regulation of photosynthetic electron transport is tightly associated with LEF in C_4 plants, similarly to C_3 plants, which is somehow unexpected if we assume that maize has a large activity of CEF. Originally, CEF in C_4 plants is hypothesized based on the biochemical fact that there is less grana structure containing PSII in the isolated bundle sheath cells. It should be noted that in this study we analysed a variety of photosynthetic parameters at the scale of intact leaves that is the mixture of mesophyll and bundle sheath cells. Here, we spectroscopically estimated the ratio of PSI to PSII *in vivo* in the intact leaves of mustard and maize. A short-saturation flash induces ECS dependent on the photochemical reaction at PSII and PSI. During far-red light illumination, where PSI is selectively excited, the short-saturation flash induces ECS presumably originated only from PSII [28]. Actually, the ECS amplitude induced by the short-saturation flash decreased with the intensity of far-red light, finally reaching approximately 50% of the initial amplitude in both mustard and maize (Fig. 9), indicating that the ratio of PSII to PSI is about 1:1 at the scale of leaves. The same results were obtained from the field-grown sunflower (C_3 plant) and maize (Supplemental Fig. S4).

To further test if there is the significant amount of PSI uncoupled from PSII in bundle sheath cells of maize, the connectivity of PSI with PSII was roughly estimated *in vivo* using a Klas-NIR spectrophotometer. A short-saturation flash was applied to excite PSII and PSI after accumulating $P700^+$ by the far-red light illumination, resulting in the decay kinetics of $P700^+$ (Fig. 10). The $P700^+$

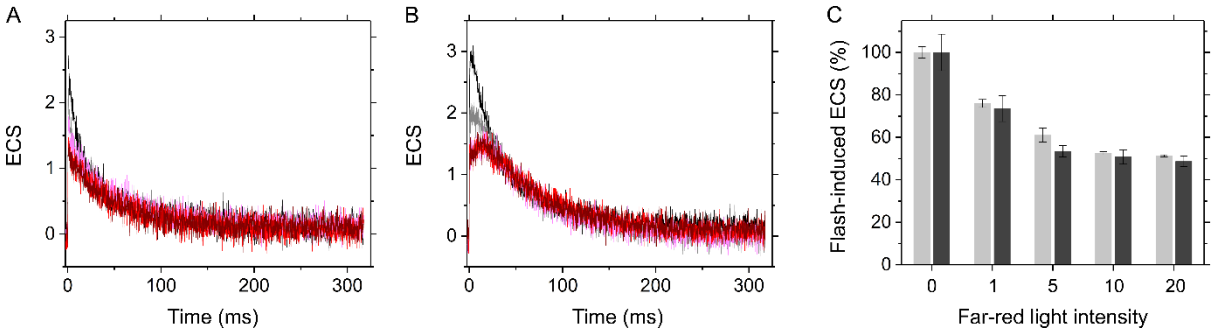

Fig. 9. Electrochromic shift (ECS) induced by a 5 µs-short saturation flash during far-red light illumination in the C_3 plant mustard (A) and the C_4 plant maize (B). Far-red light was provided at various intensities (0, black; 1, grey; 5, pink; 10, red; and the maximum 20, wine red; the values defined by the Walz software). (C) The flash-induced ECS changes normalized by the values without far-red light illumination as 100%. The data of mustard (light grey) and maize (dark grey) are shown as the mean with the standard deviation ($n = 3$, biological replicates).

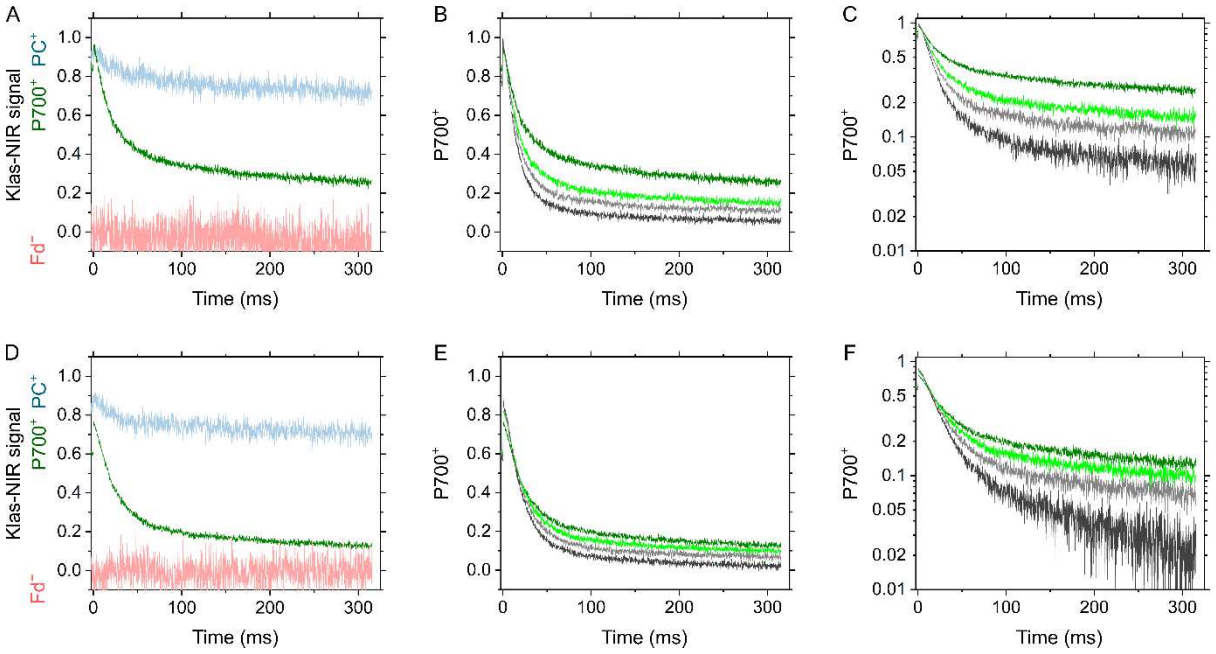

Fig. 10. Effects of a short-saturation flash on the redox state around PSI in the C_3 plant mustard (A–C) and the C_4 plant maize (D–F). (A, D) Reduction kinetics of $P700^+$ (green) in response to a 5 µs-short saturation flash after far-red light illumination for 10 s. Far-red light was provided at the maximum intensity (20, the value defined by the Walz software). Deconvoluted signals to plastocyanin (PC^+, blue) and ferredoxin (Fd^-, red) are also shown. All the Klas-NIR signals were normalized within the range from the minimum 0 to the maximum 1. The maximum reduction/oxidation levels of each component were determined as shown in Supplemental Fig. S2. The signal to Fd^- has negative values. (B, E) Reduction kinetics of $P700^+$ by a short saturation flash at different lengths (5, green; 10, light green; 20, light grey; and 50 µs, grey respectively) after far-red light illumination for 10 s. The kinetics are also shown with the logarithmic scale at y-axis (C, F). The representative traces of independent experiments ($n = 3$, biological replicates) are shown.

reduction kinetics was likely to involve in more than two components, but the rapid decay within 100 ms should reflect the electron transport from PSII [29]. Interestingly, a part of $P700^+$ (10–20%) took more than second to be reduced (data not shown), which may be due to a redox equilibration between PC and P700 as implied from the reduction of a part of PC (ca. 20%) within 100 ms (Fig. 10A and D). The redox state of Fd did not change in response to the short-saturation flash (Fig. 10A and D). The ratio of $P700^+$ rapidly reduced was rather larger in maize (ca. 80%) than in mustard (ca. 65%), both of which increased with the length of the short-saturation flash (5–50 µs) to approximately 90% (Fig. 10B, C, E, and F). These results implied that there is no significant amount of PSI having "less connectivity" with PSII uniquely to maize but not to mustard at the scale of the intact leaves. It should be noted that P700

224 was kept more reduced in maize than in mustard during far-red light illumination (Fig. 10A and D, and
225 Supplemental Fig. S2), and a part of $P700^+$ (ca. 20%) was immediately reduced within 50 μs just after
226 the illumination with 5 μs short-saturation flash (Fig. 10D), which was likely to be too fast for CEF,
227 considering the turnover of the Cyt b_6/f complex [30].

Discussion

We experimentally characterized the *in vivo* regulatory mechanisms of photosynthetic electron transport for P700 oxidation in maize, which showed the different O_2 dependency but could be understood based on the same model for C_3 plants although photosynthesis in C_4 plants is driven in co-operation of mesophyll and bundle sheath cells, and metabolically different from that in C_3 plants. Oxidation of P700 is the universal strategy for photosynthetic organisms to suppress the generation of ROS at the acceptor side of PSI, which is mainly regulated in C_3 plants by the donor-side mechanism, i.e. the ΔpH-dependent suppression of electron transport at the Cyt b_6/f complex, and by the acceptor-side one, photorespiration. Since maize did not show the enough capacity of photorespiration as an alternative electron sink, LEF was linearly suppressed with the decrease in photosynthetic CO_2 assimilation (Fig. 1). Nevertheless, P700 is kept oxidised with the suppression of CO_2 assimilation, which is linearly associated with the increase in ΔpH by limiting g_H^+ (Fig. 5). In these processes, the Fd^- oxidation rate showed the linear relationship with Y(II) (Fig. 7). The metabolic compartmentation in C_4 photosynthesis and the higher ratio of PSI to PSII in isolated bundle sheath cells have made it complicated to consider the regulation of photosynthetic electron transport in C_4 plants. However, the ratio of PSI to PSII was estimated almost 1:1 at the scale of the intact maize leaves, similarly to C_3 plants (Fig. 9). Further, the ratio of $P700^+$ rapidly reduced by a short-saturation flash was similar between mustard and maize (Fig. 10). All these results supported the robustness of P700 oxidation tightly associated with LEF in the C_4 plant maize, as previously proposed in C_3 plants, with the exception of little photorespiratory electron sink on the acceptor side of PSI [13].

Instead of the photorespiratory electron sink, maize strongly relies P700 oxidation on the ΔpH-dependent suppression of electron transport at the Cyt b_6/f complex (Fig. 2B and 5C). The decrease in g_H^+ was linearly correlated with LEF reflected in Y(II) (Fig. 5D) and Fd^- oxidation rate (Fig. 7D). These results suggest that lumen acidification for P700 oxidation was attributed to the decrease of g_H^+ but not to an additional H^+-pumping from stroma to the thylakoid lumen, for example, by CEF. The different dependencies of P700 oxidation on the regulation of g_H^+ led to the different threshold of LEF for keeping P700 oxidised between mustard and maize. Contrary to mustard, which needed about 50% of the maximum Y(II) for P700 oxidation, maize did not exhibit breakdown of P700 oxidation even when Y(II) was close to zero (Fig. 2). The linear proportional relationship between Y(II) and P700 oxidation indicated that the C_4 plant maize does not require an electron sink for P700 oxidation (Fig. 2B). The insensitivity to O_2 of P700 oxidation has been observed also at various irradiances at CO_2-saturated conditions [31]. Nevertheless, an extreme condition of 1 kPa O_2 and very low CO_2 (< 1.5 Pa) partially disturbed P700 oxidation in maize (Fig. 2B), which may be due to the slight but certain

electron flux *via* photorespiration or the Mehler reaction in C_4 plants [18, 32]. In the other word, C_4 plants ultimately utilize O_2 for P700 oxidation maybe in some extremely stressed conditions. In C_3 plants, photorespiration relieves the electron transport limitation on the acceptor side of PSI and also sustains to produce ΔpH (Fig. 2A, 5A and C, and Supplemental Fig. S1A and B). It should be trade-off to rely P700 oxidation mainly on the regulations on the donor or acceptor sides of PSI. The contribution of the regulation of g_{H^+} to P700 oxidation would be different among different types of C_4 plants and C_3-C_4 intermediates associated with the capacity of photorespiration [5]. Whereas P700 oxidation with the suppression of photosynthesis is the phenomenon commonly observed in a variety of photosynthetic organisms, the dominant molecular mechanisms are rich in diversity, which has been already diversified among different species of cyanobacteria, the progenitor of oxygenic photosynthesis [10], and has changed during the evolutionary history of photosynthetic green and red plastid lineages. Interestingly, the strategy for P700 oxidation in maize can be categorized on the view of O_2-usage into the same type of that in some secondary algae derived from red algae, which do not need O_2 for P700 oxidation [33].

What is the determinant for the strong contribution of the ΔpH-dependent donor side mechanism to P700 oxidation in maize? Lumen acidification should be controlled by both H^+-pumping and H^+-consumption rates in plant leaves. Based on the fact that the CEF activity *via* Fd was negligible (Fig. 7B and D), the H^+-pumping rate into the thylakoid lumen is estimated from LEF with the rate constant (k_{H^+}), which is correlated with Y(II). Meanwhile, the H^+-consumption rate is equal to the ECS parameter v_{H^+}, reflecting ATP consumption by CO_2 assimilation and photorespiration in C_3 plants. Finally, the change in *pmf* is presented as the following equation in C_3 plants [13]:

$$d(pmf)/dt = (k_{H^+} \times LEF) - (pmf \times g_{H^+})$$

At the steady state, $$pmf = (k_{H^+} \times LEF)/g_{H^+}$$

That is, lumen acidification occurs where LEF is sustained more than g_{H^+}. In mustard, the decrease in Y(II) (ca. 50%) was much smaller than that in g_{H^+} (ca. 85%) at 21 but not at 1 kPa O_2 (Fig. 5B), indicating that photorespiration contributes to sustaining LEF, resulting in the H^+ accumulation into the thylakoid lumen (Fig. 5A and 11)[14, 34]. In maize LEF decreased almost concomitantly with g_{H^+}, different from mustard (Fig. 5D). Nevertheless, H^+ was accumulated in the thylakoid lumen to cause P700 oxidation at both 21 and 1 kPa O_2 (Fig. 2B and 5C). Overall, different from C_3 plants, *pmf* in maize cannot be formulated as the above equation (Fig. 11). In the other words, there may be an additional mechanism to pump H^+ into the thylakoid lumen independent of the electron transport via Fd, which remains to be further investigated in future works. One possibility that cannot be excluded is the effect of the

Mehler reaction [18] on ΔpH at the steady state of photosynthesis even though the activity is very low. It should be also noted that the relationship of v_H^+ with photosynthetic CO_2 assimilation was different from that of Y(II) (Fig. 4F), which is presumably due to the different ATP consumption for regenerating PEP at various Ci. The strong contribution of the ΔpH-dependent donor side mechanism to P700 oxidation in maize should be also related to the different ATP utilization between C_3 and C_4 plants.

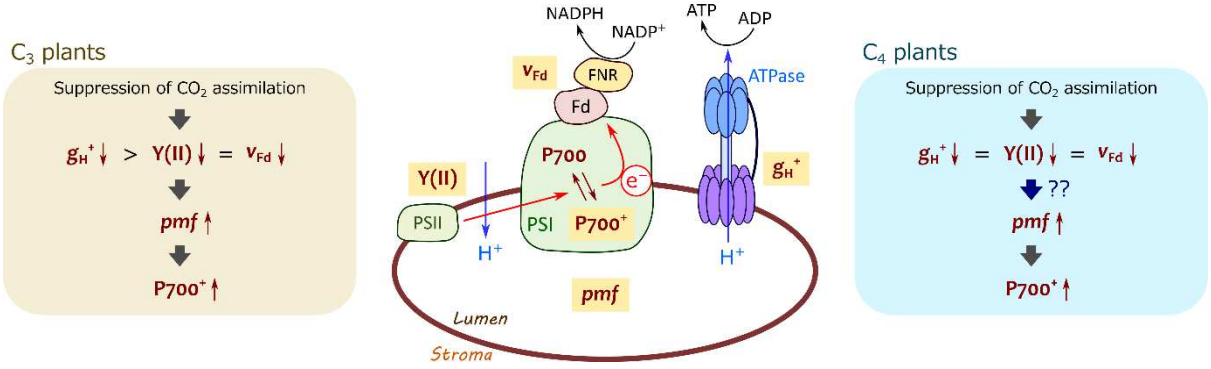

Fig. 11. A brief illustration of mechanism for P700 oxidation in C_3 and C_4 plants. In C_3 plants, proton conductance of chloroplast ATP synthase (g_H^+) decreases with the suppression of photosynthetic CO_2 assimilation greater than photosynthetic linear electron flow reflected in effective quantum yield of PSII, Y(II), and ferredoxin (Fd^-) oxidation rate (v_{Fd}), resulting in the increase in *proton motive force* (*pmf*) to induce P700 oxidation. In C_4 plants, *pmf* increases with the suppression of photosynthetic CO_2 assimilation, although g_H^+ decreases concomitantly with Y(II) and v_{Fd}.

The present results are unlikely to follow the hypothesis that CEF is driven in the bundle sheath cells of NADP-ME subtype of C_4 plants at a comparable flux to LEF in the mesophyll cells. Although there is the report that the PSII activities in the bundle sheath cells of NADP-ME subtype of C_4 plants, including maize, sorghum, and Flaveria, are almost equal to those in the mesophyll cells [35], numerous studies have followed and documented that PSII activity is nearly negligible in isolated bundle sheath cells in NADP-ME subtype of C_4 plants, especially in maize [36, 37, 38, 39, 40, 41, 42, 43], having constructed the dogma that CEF is responsible for the additional ATP production in the bundle sheath cells of C_4 plants. Actually, recent modelling studies select the CEF model for simulating C_4 photosynthesis [44]. However, it should be concerned that these studies follow the ratio of PSI to PSII in the experimentally differentiated mesophyll and bundle sheath cells, except for the semi-quantitative evaluation by immunocytology [45]. Overall, the PSI:PSII ratio has yet not been quantitatively understood at the scale of intact leaves, and there is still no evidence for the energetic contribution of CEF to photosynthesis in C_4 plants. Another problem is that *in vivo* CEF activity has been ordinarily evaluated using the effective quantum yield of PSI that is easily under/overestimated (Fig. 8)[2]. Considering the experimental results by the previous and present studies, we propose that the amount of PSI in bundle sheath cells is presumably much smaller than that in mesophyll cells at the scale of C_4 intact leaves.

It is still unclear how the additional ATP demand is met in C_4 photosynthesis. Chapman et al. (1980), one of important landmarks in C_4 photosynthesis research, has shown that in the presence of exogenously added malate photosynthetic CO_2 assimilation proceeds in the isolated bundle sheath cells of maize with PSII inhibited by 3-(3,4-dichlorophenyl)-1,1-dimethylurea (DCMU). The PSII-

independent ATP production can reach about 80% of the ATP production of the illuminated cells in the *in vitro* system [38], which clearly suggests that there is a malate-dependent ATP source in the cells. It should be also considered that the NAD(P)H dehydrogenase complex plays an important role for C_4 photosynthesis [46]. It has been recently accepted that the intermediates of the Calvin-Benson cycle shuttle between the mesophyll and bundle sheath cells with certainly large fluxes [43, 47], which can make it more complicated how much ATP and NADPH are needed respectively in these two types of cells in the light. In both mustard and maize, *pmf* was formed to some extent even in the conditions where photosynthesis and photorespiration are almost completely suppressed under 1 kPa O_2 and very low Ci (Fig. 4A and D), which suggested that ATP is, at least, not limited. We also note that the stoichiometry of ATP and NADPH may not need to be necessarily satisfied because excess NADPH should not be accumulated as long as P700 oxidation system works [2].

For the last decades, CEF has been frequently evaluated by the comparison between Y(II) and Y(I). The extra Y(I) to Y(II) has been believed to be a conventional indicator to CEF activity. Nevertheless, recently it has been clearly shown that Y(I) can be easily over-estimated by the oxidation of PC [2]. In this study, the extra Y(I) was totally coincided with the PC oxidation in both mustard and maize at various CO_2 and O_2 partial pressures (Fig. 8). These facts indicate that Y(I) must not be utilized to evaluate CEF activity. A variety of alternative methods, including the comparison of Fd^- oxidation rate with Y(II), should be considered in future works.

Materials and Methods

Plant materials

Field mustard (komatsuna, *Brassica rapa*) and maize (*Zea mays*) were grown under long-day conditions (14 h-light, 24 °C, 300 μmol photons m^{-2} s^{-1}, white fluorescent lamp/10 h-dark, 22 °C). Seeds were planted in pots that contained a 5:3:2 mix of Metro-Mix 350 (Sun Gro Horticulture, Agawam, MA, USA), Akadama, and vermiculit with 1000-fold diluted Hyponex solution (Hyponex, Osaka, Japan) used as a watering solution. For the experiments in Supplemental Fig. S4, the field-grown sunflower (*Helianthus annuus*) and maize were used.

Gas exchange, chlorophyll fluorescence, and spectroscopic analyses

Exchanges of CO_2 and H_2O were measured using a GFS-3000 equipped with a 3010-DUAL gas exchange chamber (Walz, Effeltrich, Germany) in which ambient air was saturated with water vapor at 18.0 ± 0.1 °C, and the leaf temperature was maintained at 25 ± 2 °C. Ci was calculated based on the previous report [48].

Chlorophyll fluorescence and near infrared absorbance were simultaneously measured coupled with gas exchange analysis using a Klas-NIR spectrophotometer (Walz)[49]. Chlorophyll fluorescence parameters were calculated as follows [50]: F_o, minimum fluorescence from a dark-adapted leaf; F_m', maximum fluorescence from a light-adapted leaf; F', fluorescence emission from a light-adapted leaf; $Y(II) = (F_m' - F')/F_m'$, effective quantum yield of PSII; $qL = (F_m' - F')/(F_m' - F_o') \times (F_o'/F')$, fraction of "open" PSII centres (with Q_A oxidised) on the basis of a lake model for the PSII photosynthetic apparatus; $NPQ = (F_m - F_m')/F_m'$, non-photochemical quenching. Pulse-amplitude modulated green measuring light (540 nm, <0.1 μmol photons m^{-2} s^{-1}) was used. To obtain F_m', a saturation flash (630 nm, 8,000 μmol photons m^{-2} s^{-1}, 300 ms) was applied. Red actinic light (630 nm, 550 μmol photons m^{-2} s^{-1}) was supplied using a chip-on-board LED array. The signals for $P700^+$, PC^+, and Fd^- were calculated based on the deconvolution of four pulse-modulated dual-wavelength difference signals in the near infrared region (780–820, 820–870, 840–965, and 870–965 nm). The redox state of P700 was evaluated as the ratio of $P700^+$ to the total P700, termed Y(ND) [51]. Both P700 and PC are kept completely reduced and Fd is fully oxidised in dark conditions. For the determination of total photo-oxidizable P700 and PC, the saturation flash was applied after 10 s illumination with a far-red light (740 nm; Supplemental Fig. S2)[52]. Total photo-reducible Fd was determined by the illumination with a red actinic light (450 μmol photons m^{-2} s^{-1}) after plant leaves were adapted to the dark for 5 min (Supplemental Fig. S2)[52]. For the analysis of a dark-interval relaxation kinetics, the red actinic light (550 μmol photons m^{-2} s^{-1}) was temporarily turned off for 600 ms at the steady-state

photosynthesis [27]. The oxidation rate of Fd^- was estimated as relative values by a Klas-NIR spectrophotometer by a linear fitting for the initial decay of Fd^-. Recently, it has been shown that the reduced iron-sulphur clusters in PSI, F_A/F_B, can contribute to the Klas-NIR signal attributed to Fd^- in almost the same manner *in vitro* [53]. In this study, we concluded that the F_A/F_B contribution to the Fd signal was not critical problem in the measurement for the Fd^- oxidation rate because Fd was kept oxidised more than 50% at the steady state of photosynthesis except for the condition where the electron acceptor side of PSI was extremely limited at low CO_2 and O_2 in mustard.

ECS was measured simultaneously with gas exchange using a Klas-100 spectrophotometer (Walz)[54]. The ECS signal was calculated from two pulse-modulated dual-wavelength difference signals using the following equation: $(\Delta I/I_{521.4-507.6} + \Delta I/I_{520.2-534.8})/2$. Red actinic light was temporarily turned off for 600 ms in a dark-interval relaxation kinetics analysis during the steady-state photosynthesis to determine ECS parameters [55]. The total rapid (<1 s) change in ECS signal upon rapidly switching off actinic light was defined as *pmf*. The parameter v_H^+ was estimated by a linear fitting for the initial phase of the mono-exponential decay of *pmf* in the transition from light to dark, giving the rate constant of the decay g_H^+ by the calculation. The ΔpH component of *pmf* was estimated also by turning red actinic light off for 30 s at the steady state of photosynthesis [25], which are used in Fig. 5A and C. The amplitude of ECS was normalised by the ECS change induced by a 5 µs-short saturation flash [28].

All of *in vivo* spectroscopic measurements were based on the assumption that the absorption coefficient and the amplification factor [56] of each targeted molecule are not different between mesophyll and bundle sheath cells. All statistical analyses were performed using Origin 2017 (Lightstone, Tokyo, Japan).

Funding: This work was supported by Core Research for Evolutional Science and Technology of Japan Science and Technology Agency, Japan (grant number JPMJCR1503 to C.M.) and by Japan Society for the Promotion of Science (grant number 16J03443 to G.S.).

Disclosures: Conflict of interest: No conflict of interest declared.

Acknowledgements: The authors gratefully thank Dr. Pierre Sétif and Dr. Anja Krieger-Liszkay for their kind advices in writing the manuscript. The authors also thank Editage (www.editage.jp) for providing English corrections.

403 **Figure legends**

404

405 **Fig. 1.** Photosynthetic CO_2 assimilation and linear electron flow in the C_3 plant mustard (A−C) and the
406 C_4 plant maize (D−F). (A, D) Net CO_2 assimilation rate at various intercellular CO_2 partial pressures (Ci).
407 (B, E) Effective quantum yield of PSII, Y(II), at various Ci. (C, F) Relationship of Y(II) with CO_2 assimilation
408 rate. Dark respiration rate is presented as Rd. Experiments were conducted independently three times
409 as shown in different symbols (biological replicates) at 21 kPa (closed symbols) and 1 kPa O_2 (open
410 symbols). Solid lines represent estimated linear regression of the data at 1 kPa (C) and 21 kPa O_2 (F)
411 (R^2, coefficient of determination). The *y*-intercepts (*b*) were tested based on the null hypothesis:
412 $^{**}p<0.005$.

413

414 **Fig. 2.** Relationship of P700 oxidation with effective quantum yield of PSII, Y(II), at various intercellular
415 CO_2 partial pressures in the C_3 plant mustard (A) and the C_4 plant maize (B). Experiments were
416 conducted independently three times as shown in different symbols (biological replicates) at 21 kPa
417 (closed symbols) and 1 kPa O_2 (open symbols). Solid lines represent estimated linear regression of the
418 data at 21 kPa O_2 (R^2, coefficient of determination).

419

420 **Fig. 3.** Dark-interval relaxation kinetics of electrochromic shift (ECS) in the C_3 plant mustard (A) and
421 the C_4 plant maize (B) under ambient air (40 Pa CO_2, 21 kPa O_2; black), low CO_2 (1 Pa CO_2, 21 kPa O_2;
422 purple), and low CO_2/O_2 (1 Pa CO_2, 1 kPa O_2; pink). Red actinic light (550 µmol photons m^{-2} s^{-1}) was
423 turned off at 0 ms for 600 ms during the steady-state photosynthesis. The kinetics were fit to mono
424 exponential decay (R^2, coefficient of determination: 0.7017, 0.9454, and 0.6868 in A; 0.8814, 9868,
425 and 0.9801 in B respectively).

426

427 **Fig. 4.** Electrochromic shift (ECS) parameters in the C_3 plant mustard (A−C) and the C_4 plant maize
428 (D−F). (A, D) *Proton motive force* (*pmf*) at various intercellular CO_2 partial pressures (Ci). (B, E) Proton
429 conductance of the chloroplast ATP synthase (g_{H^+}) at various Ci. (C, F) Relationship of proton efflux
430 rate *via* the ATP synthase (v_{H^+}) with CO_2 assimilation rate. Effective quantum yield of PSII, Y(II), are also
431 shown in orange symbols. Dark respiration rate is presented as Rd. Experiments were conducted
432 independently three times as shown in different symbols (biological replicates) at 21 kPa (closed
433 symbols) and 1 kPa O_2 (open symbols).

434

435 **Fig. 5.** Relationships of the proton gradient across the thylakoid membrane (ΔpH; A, C) and the proton
436 conductance of the chloroplast ATP synthase (g_{H^+}; B, D) with effective quantum yield of PSII, Y(II), at

various intercellular CO_2 partial pressures in the C_3 plant mustard (A, B) and the C_4 plant maize (C, D). We note that ΔpH and g_{H^+} were separately measured from Y(II) at the same ambient CO_2 partial pressures. Experiments were conducted independently three times as shown in different symbols (biological replicates) at 21 kPa (closed symbols) and 1 kPa O_2 (open symbols). Solid lines represent estimated linear regression of the data at 21 kPa O_2 (R^2, coefficient of determination).

Fig. 6. Dark-interval relaxation kinetics of ferredoxin (Fd^-) in the C_3 plant mustard (A) and the C_4 plant maize (B) under ambient air (40 Pa CO_2, 21 kPa O_2; black), low CO_2 (1 Pa CO_2, 21 kPa O_2; purple), and low CO_2/O_2 (1 Pa CO_2, 1 kPa O_2; pink). Red actinic light (550 µmol photons m^{-2} s^{-1}) was turned off at 0 ms for 600 ms during the steady-state photosynthesis. The kinetics were fit to mono exponential decay (R^2, coefficient of determination: 0.6628, 0.8816, and 0.9788 in A; 0.6612 and 0.8307 in B). Only Fd^- kinetics in maize under low CO_2/O_2 was fit to biphasic exponential decay (R^2: 0.9405).

Fig. 7. *In vivo* measurement for the redox state of ferredoxin (Fd) in the C_3 plant mustard (A, B) and the C_4 plant maize (C, D). (A, C) The Fd reduction during the steady-state photosynthesis at various intercellular CO_2 partial pressures (Ci). (B, D) Relationship of Fd^- oxidation rate with effective quantum yield of PSII, Y(II), at various Ci. Experiments were conducted independently three times as shown in different symbols (biological replicates) at 21 kPa (closed symbols) and 1 kPa O_2 (open symbols). Solid lines represent the estimated linear regressions of the data at 1 kPa (B) and 21 kPa O_2 (D), respectively (R^2, coefficient of determination). The *y*-intercepts (*b*) were tested based on the null hypothesis: $^{\#}p>0.05$.

Fig. 8. Relationships of effective quantum yield of PSI, Y(I) (A, C), and plastocyanin (PC) oxidation (B, D) with effective quantum yield of PSII, Y(II), at various intercellular CO_2 partial pressures in the C_3 plant mustard (A, B) and the C_4 plant maize (C, D). Experiments were conducted independently three times as shown in different symbols (biological replicates) at 21 kPa (closed symbols) and 1 kPa O_2 (open symbols).

Fig. 9. Electrochromic shift (ECS) induced by a 5 µs-short saturation flash during far-red light illumination in the C_3 plant mustard (A) and the C_4 plant maize (B). Far-red light was provided at various intensities (0, black; 1, grey; 5, pink; 10, red; and the maximum 20, wine red; the values defined by the Walz software). (C) The flash-induced ECS changes normalized by the values without far-red light illumination as 100%. The data of mustard (light grey) and maize (dark grey) are shown as the mean with the standard deviation (*n* = 3, biological replicates).

Fig. 10. Effects of a short-saturation flash on the redox state around PSI in the C_3 plant mustard (A–C) and the C_4 plant maize (D–F). (A, D) Reduction kinetics of $P700^+$ (green) in response to a 5 μs-short saturation flash after far-red light illumination for 10 s. Far-red light was provided at the maximum intensity (20, the value defined by the Walz software). Deconvoluted signals to plastocyanin (PC^+, blue) and ferredoxin (Fd^-, red) are also shown. All the Klas-NIR signals were normalized within the range from the minimum 0 to the maximum 1. The maximum reduction/oxidation levels of each component were determined as shown in Supplemental Fig. S2. The signal to Fd^- has negative values. (B, E) Reduction kinetics of $P700^+$ by a short saturation flash at different lengths (5, green; 10, light green; 20, light grey; and 50 μs, grey respectively) after far-red light illumination for 10 s. The kinetics are also shown with the logarithmic scale at *y*-axis (C, F). The representative traces of independent experiments (n = 3, biological replicates) are shown.

Fig. 11. A brief illustration of mechanism for P700 oxidation in C_3 and C_4 plants. In C_3 plants, proton conductance of chloroplast ATP synthase (g_{H^+}) decreases with the suppression of photosynthetic CO_2 assimilation greater than photosynthetic linear electron flow reflected in effective quantum yield of PSII, Y(II), and ferredoxin (Fd^-) oxidation rate (v_{Fd}), resulting in the increase in *proton motive force* (*pmf*) to induce P700 oxidation. In C_4 plants, *pmf* increases with the suppression of photosynthetic CO_2 assimilation, although g_{H^+} decreases concomitantly with Y(II) and v_{Fd}.

References

1. Farquhar GD, von Caemmerer S, Berry JA. A biochemical model of photosynthetic CO_2 assimilation in leaves of C_3 species. *Planta* **149**, 78-90 (1980).

2. Furutani R*, et al.* P700 oxidation suppresses the production of reactive oxygen species in photosystem I. In: *Advances in Botanical Research*). Academic Press (2020).

3. Morales A*, et al.* In silico analysis of the regulation of the photosynthetic electron transport chain in C_3 plants. *Plant Physiol* **176**, 1247-1261 (2018).

4. Devi MT, Raghavendra AS. Photorespiration in C_3–C_4 intermediate species of *Alternanthera* and *Parthenium*: Reduced ammonia production and increased capacity of CO_2 refixation in the light. *Photosynth Res* **38**, 177-184 (1993).

5. Hanawa H*, et al.* Land plants drive photorespiration as higher electron-sink: comparative study of post-illumination transient O_2-uptake rates from liverworts to angiosperms through ferns and gymnosperms. *Physiol Plant* **161**, 138-149 (2017).

6. Stitt M, Heldt HW. Generation and maintenance of concentration gradients between the mesophyll and bundle sheath in maize leaves. *Biochim Biophys Acta Bioenerg* **808**, 400-414 (1985).

7. Osmond CB. Photorespiration and photoinhibition: Some implications for the energetics of photosynthesis. *Biochim Biophys Acta Bioenerg* **639**, 77-98 (1981).

8. Laisk A, Edwards GE. A mathematical model of C_4 photosynthesis: The mechanism of concentrating CO_2 in NADP-malic enzyme type species. *Photosynth Res* **66**, 199 (2000).

9. Sejima T, Takagi D, Fukayama H, Makino A, Miyake C. Repetitive short-pulse light mainly inactivates photosystem I in sunflower leaves. *Plant Cell Physiol* **55**, 1184-1193 (2014).

10. Shimakawa G, Shaku K, Miyake C. Oxidation of P700 in photosystem I is essential for the growth of cyanobacteria. *Plant Physiol* **172**, 1443-1450 (2016).

11. Shimakawa G, Miyake C. Oxidation of P700 ensures robust photosynthesis. *Front Plant Sci* **9**, 1617 (2018).

12. Foyer C, Furbank R, Harbinson J, Horton P. The mechanisms contributing to photosynthetic control of electron transport by carbon assimilation in leaves. *Photosynth Res* **25**, 83-100 (1990).

13. Miyake C. Molecular mechanism of oxidation of P700 and suppression of ros production in photosystem I in response to electron-sink limitations in C_3 plants. *Antioxidants* **9**, 230 (2020).

14. Wada S, Suzuki Y, Miyake C. Photorespiration enhances acidification of the thylakoid lumen, reduces the plastoquinone pool, and contributes to the oxidation of P700 at a lower partial pressure of CO_2 in wheat leaves. *Plants* **9**, (2020).

15. Sejima T*, et al.* Post-illumination transient O_2-uptake is driven by photorespiration in tobacco leaves. *Physiol Plant* **156**, 227-238 (2016).

16. Allen JF. Photosynthesis of ATP-electrons, proton pumps, rotors, and poise. *Cell* **110**, 273-276 (2002).

17. Krall JP, Edwards GE. Relationship between photosystem II activity and CO_2 fixation in leaves. *Physiol Plant* **86**, 180-187 (1992).

18. Laisk A, Edwards GE. Oxygen and electron flow in C_4 photosynthesis: Mehler reaction, photorespiration and CO_2 concentration in the bundle sheath. *Planta* **205**, 632-645 (1998).

19. Maroco JP, Ku MSB, Edwards GE. Oxygen sensitivity of C_4 photosynthesis: evidence from gas exchange and chlorophyll fluorescence analyses with different C_4 subtypes. *Plant Cell Environ* **20**, 1525-1533 (1997).

20. Oberhuber W, Dai Z-Y, Edwards GE. Light dependence of quantum yields of Photosystem II and CO_2 fixation in C_3 and C_4 plants. *Photosynth Res* **35**, 265-274 (1993).

21. Genty B, Briantais J-M, Baker NR. The relationship between the quantum yield of photosynthetic electron transport and quenching of chlorophyll fluorescence. *Biochim Biophys Acta, Gen Subj* **990**, 87-92 (1989).

22. Driever SM, Baker NR. The water–water cycle in leaves is not a major alternative electron sink for dissipation of excess excitation energy when CO_2 assimilation is restricted. *Plant Cell Environ* **34**, 837-846 (2011).

23. Kanazawa A, Kramer DM. In vivo modulation of nonphotochemical exciton quenching (NPQ) by regulation of the chloroplast ATP synthase. *Proc Natl Acad Sci USA* **99**, 12789-12794 (2002).

24. Avenson TJ, Cruz JA, Kanazawa A, Kramer DM. Regulating the proton budget of higher plant photosynthesis. *Proc Natl Acad Sci USA* **102**, 9709-9713 (2005).

25. Cruz JA, Sacksteder CA, Kanazawa A, Kramer DM. Contribution of electric field (Δψ) to steady-state transthylakoid proton motive force (*pmf*) *in vitro* and *in vivo*. Control of *pmf* parsing into Δψ and ΔpH by ionic strength. *Biochemistry* **40**, 1226-1237 (2001).

26. Ruban AV. The Mechanism of Nonphotochemical Quenching: The End of the Ongoing Debate. *Plant Physiol* **181**, 383-384 (2019).

27. Kadota K, Furutani R, Makino A, Suzuki Y, Wada S, Miyake C. Oxidation of P700 induces alternative electron flow in photosystem I in wheat leaves. *Plants* **8**, 152 (2019).

28. Klughammer C, Siebke K, Schreiber U. Continuous ECS-indicated recording of the proton-motive charge flux in leaves. *Photosynth Res* **117**, 471-487 (2013).

29. Oja V, Eichelmann H, Peterson RB, Rasulov B, Laisk A. Deciphering the 820 nm signal: redox state of donor side and quantum yield of Photosystem I in leaves. *Photosynth Res* **78**, 1 (2003).

30. Buchert F, Mosebach L, Gäbelein P, Hippler M. PGR5 is required for efficient Q cycle in the cytochrome b_6f complex during cyclic electron flow. *Biochem J* **477**, 1631-1650 (2020).

31. Peterson RB. Regulation of electron transport in photosystems I and II in C_3, C_3-C_4, and C_4 species of *Panicum* in response to changing irradiance and O_2 levels. *Plant Physiol* **105**, 349-356 (1994).

32. Zelitch I, Schultes NP, Peterson RB, Brown P, Brutnell TP. High glycolate oxidase activity is required for survival of maize in normal air. *Plant Physiol* **149**, 195-204 (2009).

33. Shimakawa G, Murakami A, Niwa K, Matsuda Y, Wada A, Miyake C. Comparative analysis of strategies to prepare electron sinks in aquatic photoautotrophs. *Photosynth Res* **139**, 401-411 (2019).

34. Furutani R, Makino A, Suzuki Y, Wada S, Shimakawa G, Miyake C. Intrinsic fluctuations in transpiration induce photorespiration to oxidize P700 in photosystem I. *Plants* **9**, 1761 (2020).

35. Nakano Y, Edwards GE. Hill reaction, hydrogen peroxide scavenging, and ascorbate peroxidase activity of mesophyll and bundle sheath chloroplasts of NADP-malic enzyme type C_4 species. *Plant Physiol* **85**, 294-298 (1987).

36. Woo KC, Anderson JM, Boardman NK, Downton WJS, Osmond CB, Thorne SW. Deficient photosystem II in agranal bundle sheath chloroplasts of C_4 plants. *Proc Natl Acad Sci USA* **67**, 18-25 (1970).

37. Gutierrez M, Gracen VE, Edwards GE. Biochemical and cytological relationships in C_4 plants. *Planta* **119**, 279-300 (1974).

38. Chapman KSR, Berry JA, Hatch MD. Photosynthetic metabolism in bundle sheath cells of the C_4 species *Zea mays*: Sources of ATP and NADPH and the contribution of photosystem II. *Arch Biochem Biophys* **202**, 330-341 (1980).

39. Ivanov B, Asada K, Kramer DM, Edwards G. Characterization of photosynthetic electron transport in bundle sheath cells of maize. I. Ascorbate effectively stimulates cyclic electron flow around PSI. *Planta* **220**, 572-581 (2005).

40. Pfündel E, Nagel E, Meister A. Analyzing the light energy distribution in the photosynthetic apparatus of C_4 plants using highly purified mesophyll and bundle-sheath thylakoids. *Plant Physiol* **112**, 1055-1070 (1996).

41. Majeran W, Zybailov B, Ytterberg AJ, Dunsmore J, Sun Q, van Wijk KJ. Consequences of C_4 differentiation for chloroplast membrane proteomes in maize mesophyll and bundle sheath cells. *Mol Cell Proteomics* **7**, 1609-1638 (2008).

42. Romanowska E, Drożak A, Pokorska B, Shiell BJ, Michalski WP. Organization and activity of photosystems in the mesophyll and bundle sheath chloroplasts of maize. *J Plant Physiol* **163**, 607-618 (2006).

43. Pick TR*, et al.* Systems analysis of a maize leaf developmental gradient redefines the current C_4 model and provides candidates for regulation. *Plant Cell* **23**, 4208-4220 (2011).

44. Yin X, Struik PC. The energy budget in C_4 photosynthesis: insights from a cell-type-specific electron transport model. *New Phytol* **218**, 986-998 (2018).

45. Robertson EJ, Baker NR, Leech RM. Chloroplast thylakoid protein changes induced by low growth temperature in maize revealed by immunocytology. *Plant Cell Environ* **16**, 809-818 (1993).

46. Peterson RB, Schultes NP, McHale NA, Zelitch I. Evidence for a role for NAD(P)H dehydrogenase in concentration of CO_2 in the bundle sheath cell of *Zea mays*. *Plant Physiol* **171**, 125-138 (2016).

47. Friso G, Majeran W, Huang M, Sun Q, van Wijk KJ. Reconstruction of metabolic pathways, protein expression, and homeostasis machineries across maize bundle sheath and mesophyll chloroplasts: Large-scale quantitative proteomics using the first maize genome assembly. *Plant Physiol* **152**, 1219-1250 (2010).

48. von Caemmerer S, Farquhar GD. Some relationships between the biochemistry of photosynthesis and the gas exchange of leaves. *Planta* **153**, 376-387 (1981).

49. Klughammer C, Schreiber U. Deconvolution of ferredoxin, plastocyanin, and P700 transmittance changes in intact leaves with a new type of kinetic LED array spectrophotometer. *Photosynth Res* **128**, 195-214 (2016).

50. Baker NR. Chlorophyll fluorescence: a probe of photosynthesis in vivo. *Annu Rev Plant Biol* **59**, 89-113 (2008).

51. Klughammer C, Schreiber U. An improved method, using saturating light pulses, for the determination of photosystem I quantum yield via $P700^{+}$-absorbance changes at 830 nm. *Planta* **192**, 261-268 (1994).

52. Schreiber U. Redox changes of ferredoxin, P700, and plastocyanin measured simultaneously in intact leaves. *Photosynth Res* **134**, 343-360 (2017).

53. Sétif P, Boussac A, Krieger-Liszkay A. Near infrared *in vitro* measurements of photosystem I cofactors and electron-transfer partners with a recently-developed spectrophotometer. *Photosynth Res* **In press**, (2019).

54. Klughammer C, Kolbowski J, Schreiber U. LED array spectrophotometer for measurement of time resolved difference spectra in the 530–600 nm wavelength region. *Photosynth Res* **25**, 317-327 (1990).

55. Sacksteder CA, Kramer DM. Dark-interval relaxation kinetics (DIRK) of absorbance changes as a quantitative probe of steady-state electron transfer. *Photosynth Res* **66**, 145-158 (2000).

56. Shimakawa G, Sétif P, Krieger-Liszkay A. Near-infrared in vivo measurements of photosystem I and its lumenal electron donors with a recently developed spectrophotometer. *Photosynth Res* **144**, 63-72 (2020).

Figures

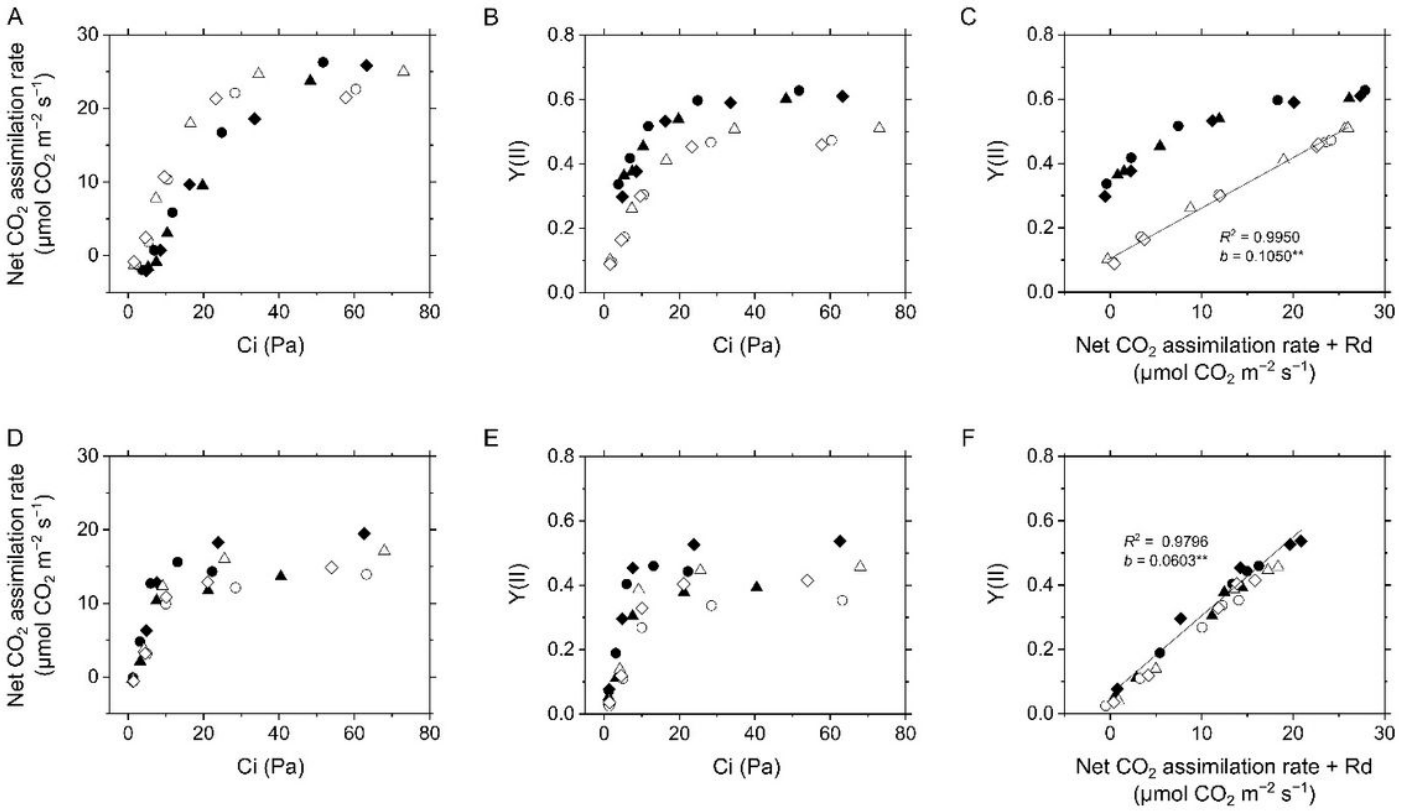

Figure 1

Photosynthetic CO2 assimilation and linear electron flow in the C3 plant mustard (A–C) and the C4 plant maize (D–F). (A, D) Net CO2 assimilation rate at various intercellular CO2 partial pressures (Ci). (B, E) Effective quantum yield of PSII, Y(II), at various Ci. (C, F) Relationship of Y(II) with CO2 assimilation rate. Dark respiration rate is presented as Rd. Experiments were conducted independently three times as shown in different symbols (biological replicates) at 21 kPa (closed symbols) and 1 kPa O2 (open symbols). Solid lines represent estimated linear regression of the data at 1 kPa (C) and 21 kPa O2 (F) (R2, coefficient of determination). The y-intercepts (b) were tested based on the null hypothesis: **p<0.005.

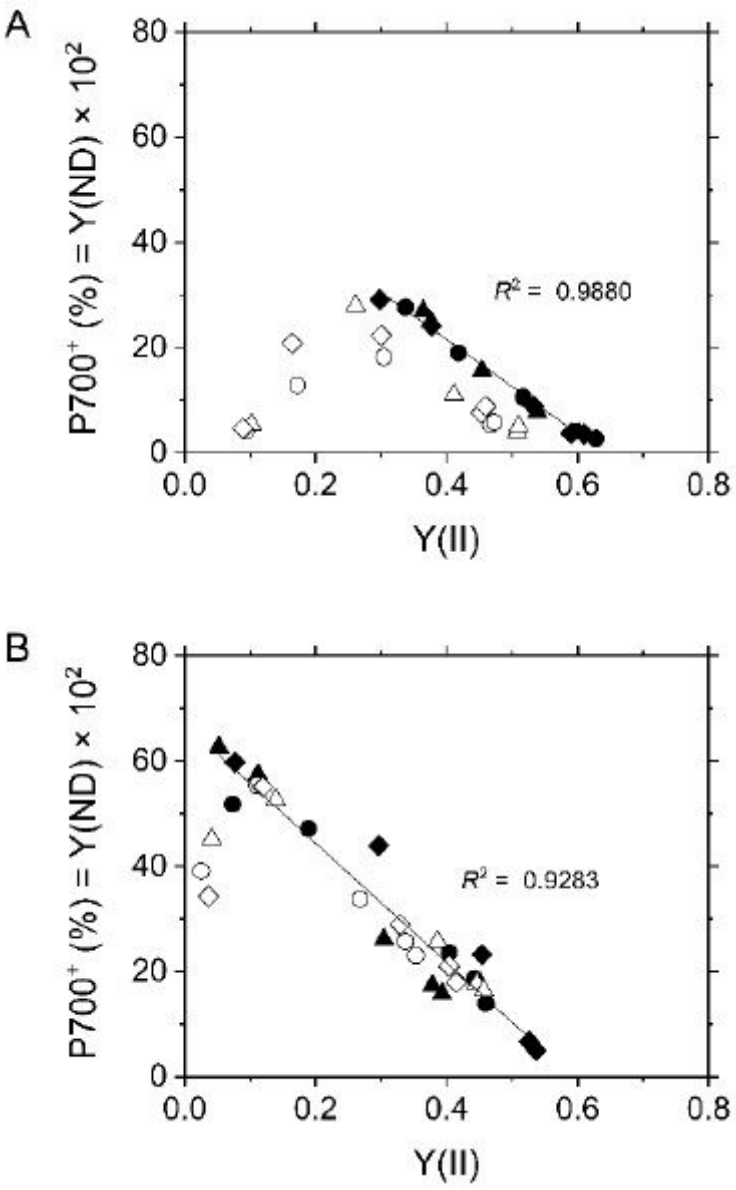

Figure 2

Relationship of P700 oxidation with effective quantum yield of PSII, Y(II), at various intercellular CO2 partial pressures in the C3 plant mustard (A) and the C4 plant maize (B). Experiments were conducted independently three times as shown in different symbols (biological replicates) at 21 kPa (closed symbols) and 1 kPa O2 (open symbols). Solid lines represent estimated linear regression of the data at 21 kPa O2 (R2, coefficient of determination).

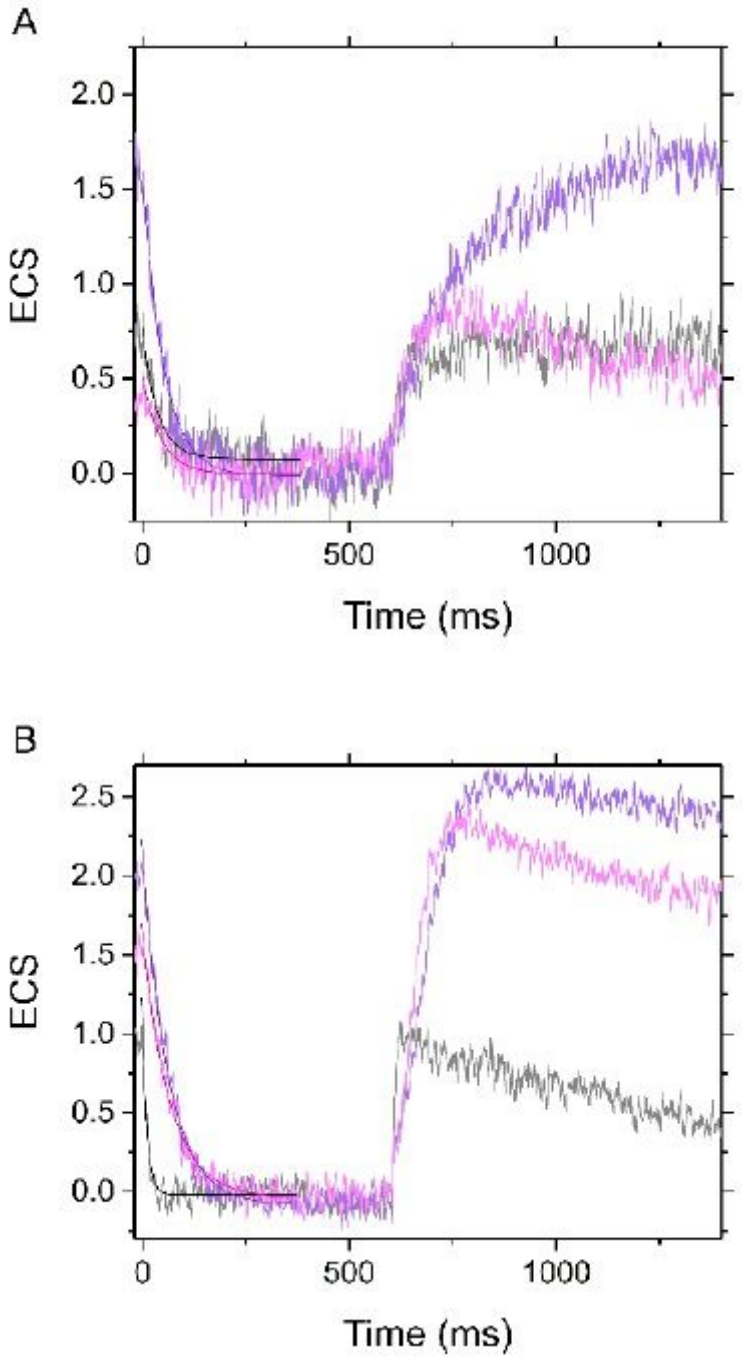

Figure 3

Dark-interval relaxation kinetics of electrochromic shift (ECS) in the C3 plant mustard (A) and the C4 plant maize (B) under ambient air (40 Pa CO2, 21 kPa O2; black), low CO2 (1 Pa CO2, 21 kPa O2; purple), and low CO2/O2 (1 Pa CO2, 1 kPa O2; pink). Red actinic light (550 µmol photons m−2 s−1) was turned off at 0 ms for 600 ms during the steady-state photosynthesis. The kinetics were fit to mono exponential decay (R2, coefficient of determination: 0.7017, 0.9454, and 0.6868 in A; 0.8814, 9868, and 0.9801 in B respectively).

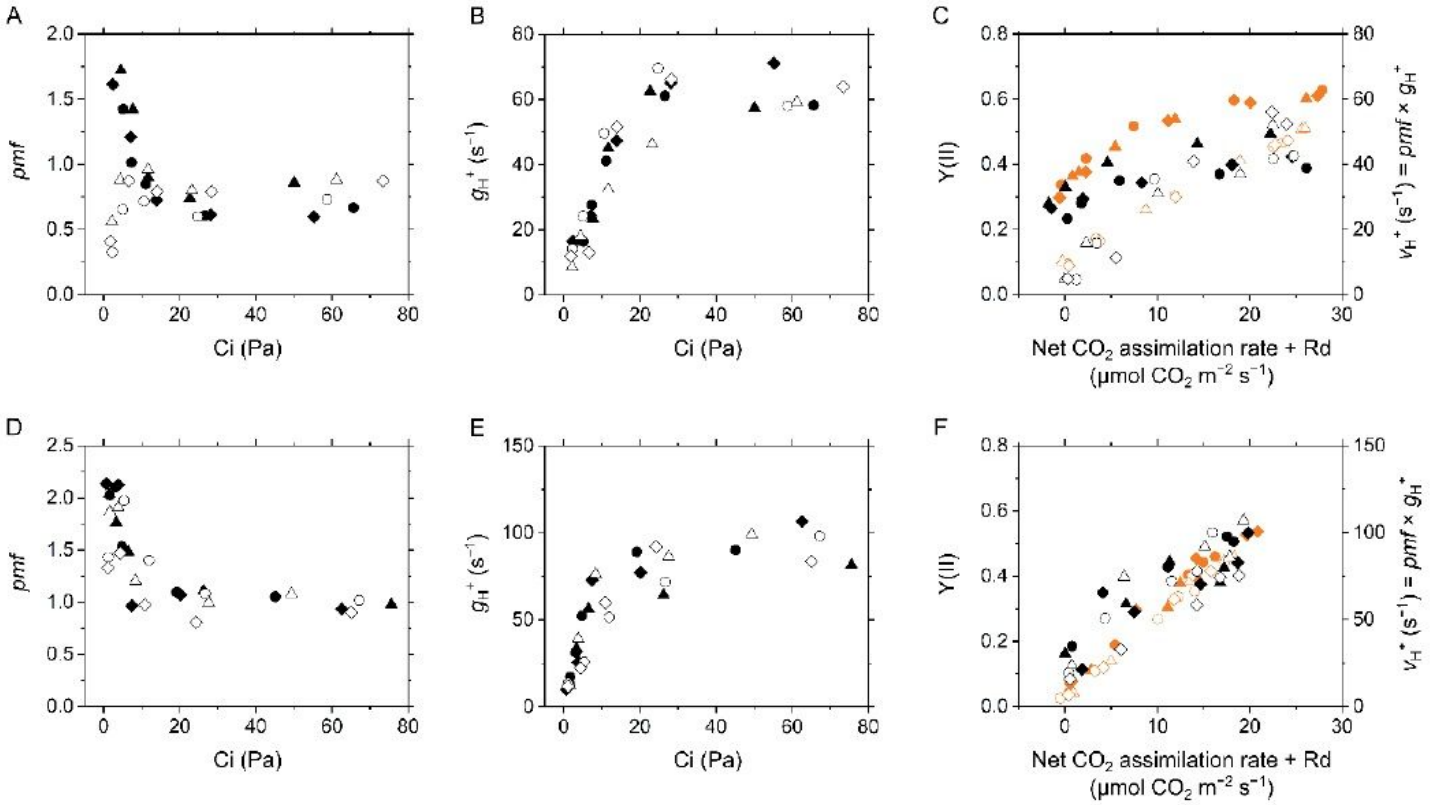

Figure 4

Electrochromic shift (ECS) parameters in the C3 plant mustard (A–C) and the C4 plant maize (D–F). (A, D) Proton motive force (pmf) at various intercellular CO2 partial pressures (Ci). (B, E) Proton conductance of the chloroplast ATP synthase (gH+) at various Ci. (C, F) Relationship of proton efflux rate via the ATP synthase (vH+) with CO2 assimilation rate. Effective quantum yield of PSII, Y(II), are also shown in orange symbols. Dark respiration rate is presented as Rd. Experiments were conducted independently three times as shown in different symbols (biological replicates) at 21 kPa (closed symbols) and 1 kPa O2 (open symbols).

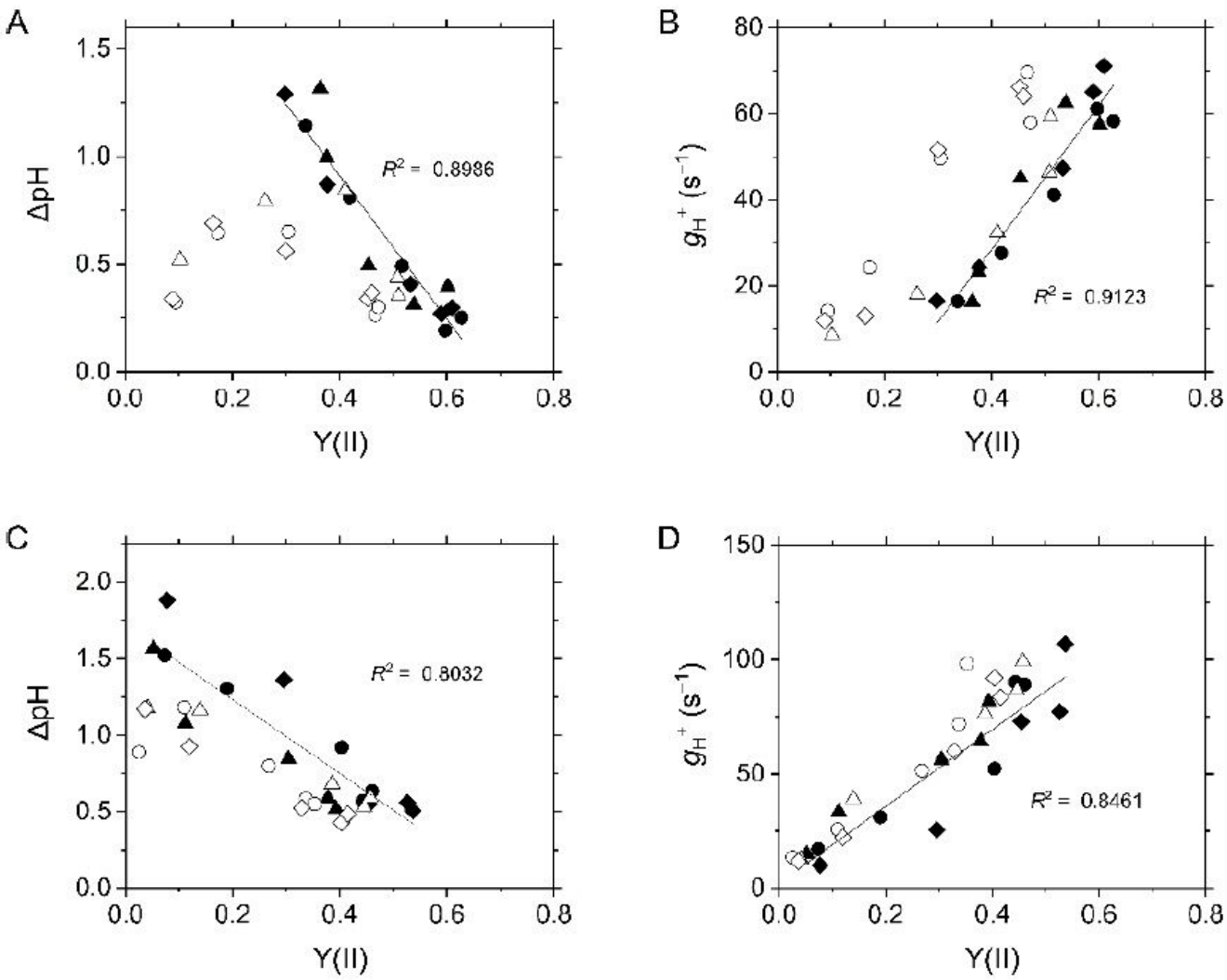

Figure 5

Relationships of the proton gradient across the thylakoid membrane (ΔpH; A, C) and the proton conductance of the chloroplast ATP synthase (gH+; B, D) with effective quantum yield of PSII, Y(II), at various intercellular CO2 partial pressures in the C3 plant mustard (A, B) and the C4 plant maize (C, D). We note that ΔpH and gH+ were separately measured from Y(II) at the same ambient CO2 partial pressures. Experiments were conducted independently three times as shown in different symbols (biological replicates) at 21 kPa (closed symbols) and 1 kPa O2 (open symbols). Solid lines represent estimated linear regression of the data at 21 kPa O2 (R2, coefficient of determination).

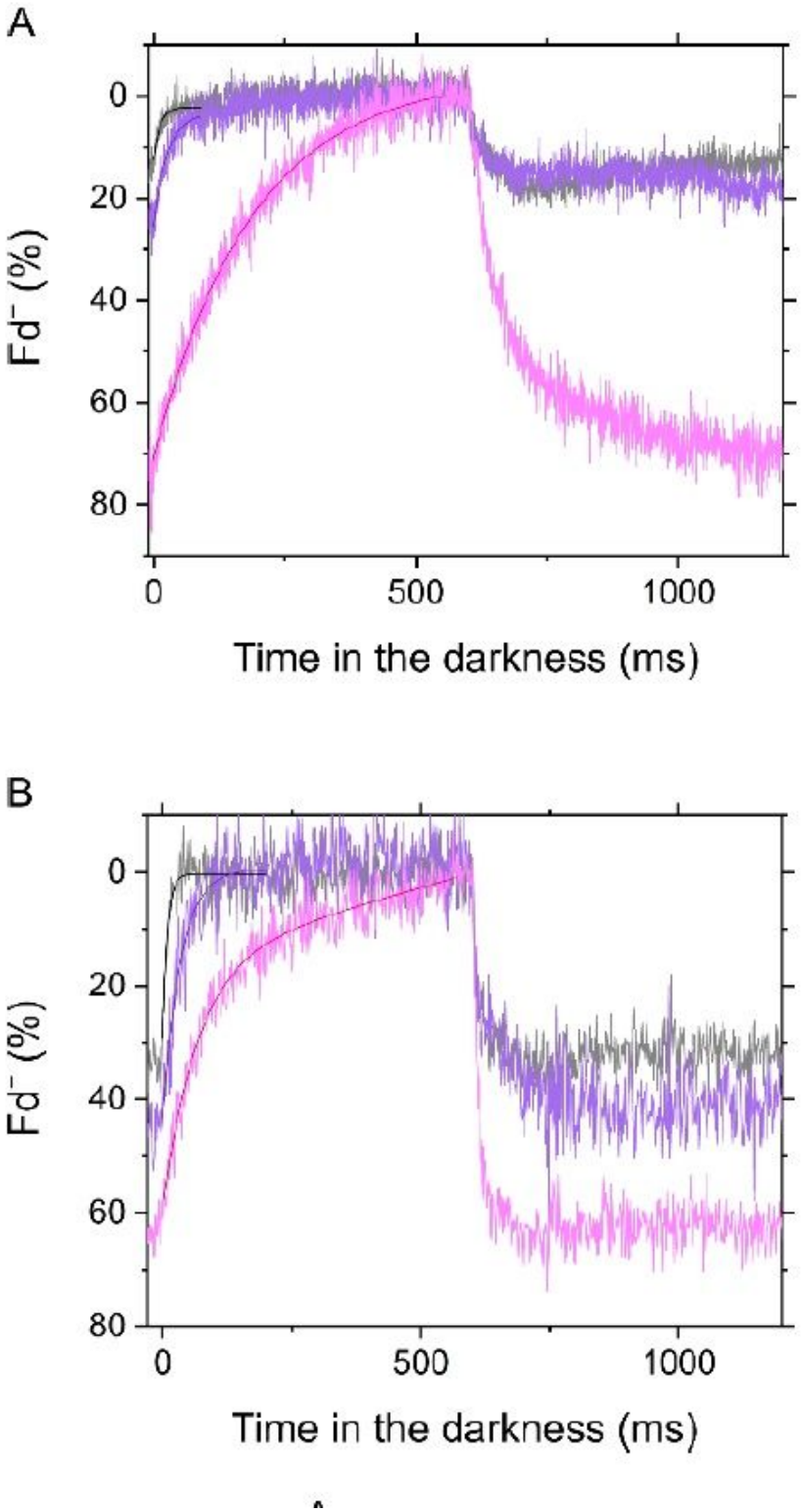

Figure 6

Dark-interval relaxation kinetics of ferredoxin (Fd−) in the C3 plant mustard (A) and the C4 plant maize (B) under ambient air (40 Pa CO2, 21 kPa O2; black), low CO2 (1 Pa CO2, 21 kPa O2; purple), and low CO2/O2 (1 Pa CO2, 1 kPa O2; pink). Red actinic light (550 µmol photons m−2 s−1) was turned off at 0 ms for 600 ms during the steady-state photosynthesis. The kinetics were fit to mono exponential decay (R2,

coefficient of determination: 0.6628, 0.8816, and 0.9788 in A; 0.6612 and 0.8307 in B). Only Fd− kinetics in maize under low CO2/O2 was fit to biphasic exponential decay (R2: 0.9405).

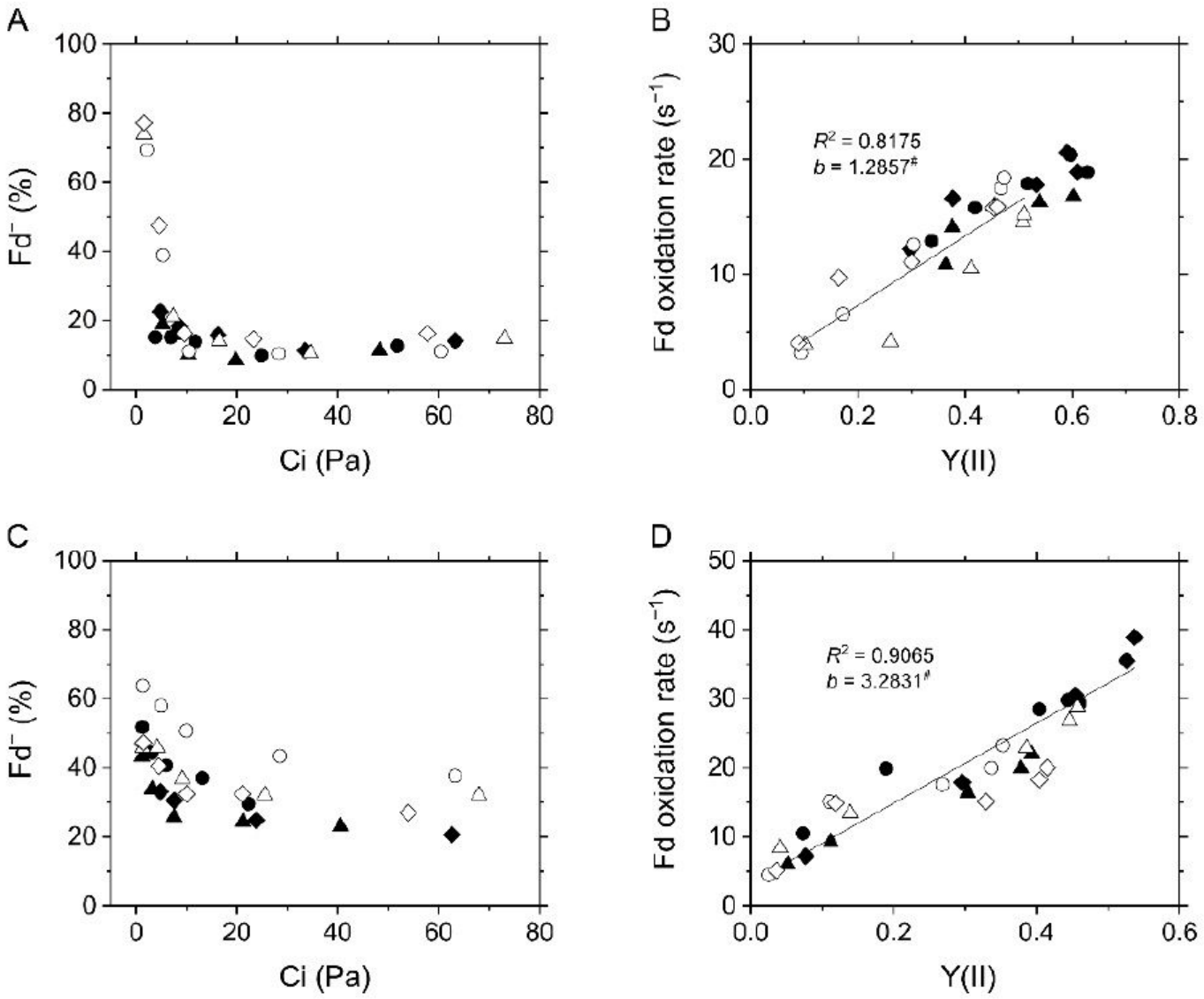

Figure 7

In vivo measurement for the redox state of ferredoxin (Fd) in the C3 plant mustard (A, B) and the C4 plant maize (C, D). (A, C) The Fd reduction during the steady-state photosynthesis at various intercellular CO2 partial pressures (Ci). (B, D) Relationship of Fd− oxidation rate with effective quantum yield of PSII, Y(II), at various Ci. Experiments were conducted independently three times as shown in different symbols (biological replicates) at 21 kPa (closed symbols) and 1 kPa O2 (open symbols). Solid lines represent the estimated linear regressions of the data at 1 kPa (B) and 21 kPa O2 (D), respectively (R2, coefficient of determination). The y-intercepts (b) were tested based on the null hypothesis: #p>0.05.

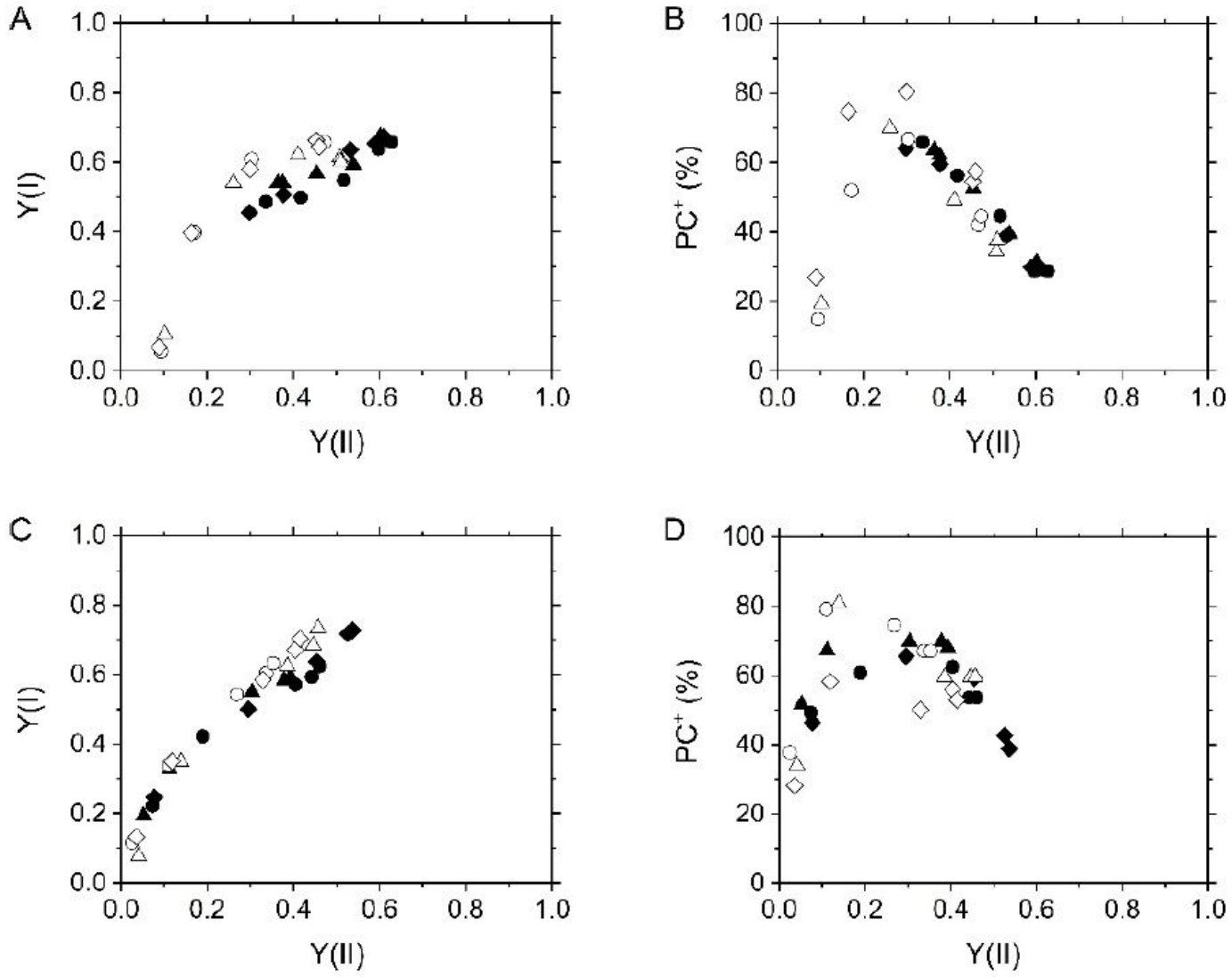

Figure 8

Relationships of effective quantum yield of PSI, Y(I) (A, C), and plastocyanin (PC) oxidation (B, D) with effective quantum yield of PSII, Y(II), at various intercellular CO2 partial pressures in the C3 plant mustard (A, B) and the C4 plant maize (C, D). Experiments were conducted independently three times as shown in different symbols (biological replicates) at 21 kPa (closed symbols) and 1 kPa O2 (open symbols).

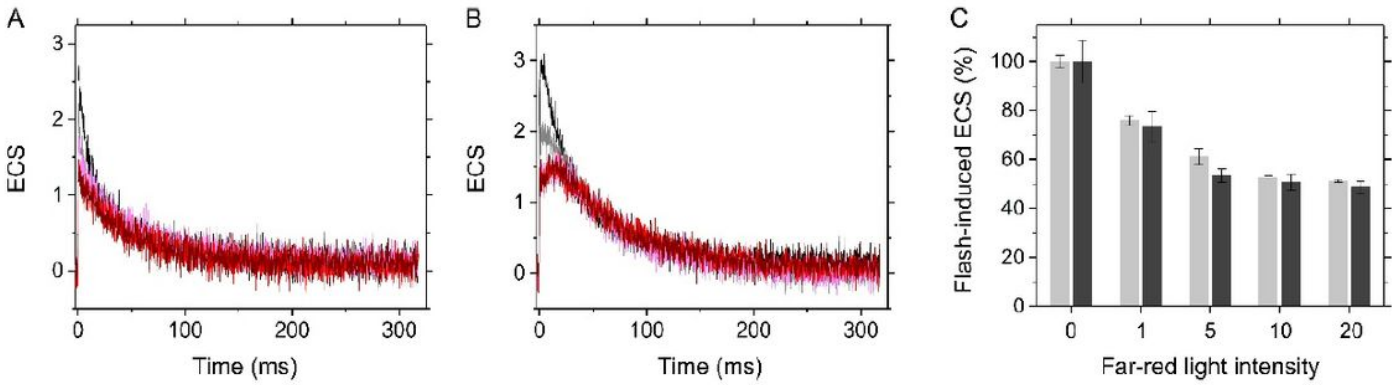

Figure 9

Electrochromic shift (ECS) induced by a 5 µs-short saturation flash during far-red light illumination in the C3 plant mustard (A) and the C4 plant maize (B). Far-red light was provided at various intensities (0, black; 1, grey; 5, pink; 10, red; and the maximum 20, wine red; the values defined by the Walz software). (C) The flash-induced ECS changes normalized by the values without far-red light illumination as 100%. The data of mustard (light grey) and maize (dark grey) are shown as the mean with the standard deviation (n = 3, biological replicates).

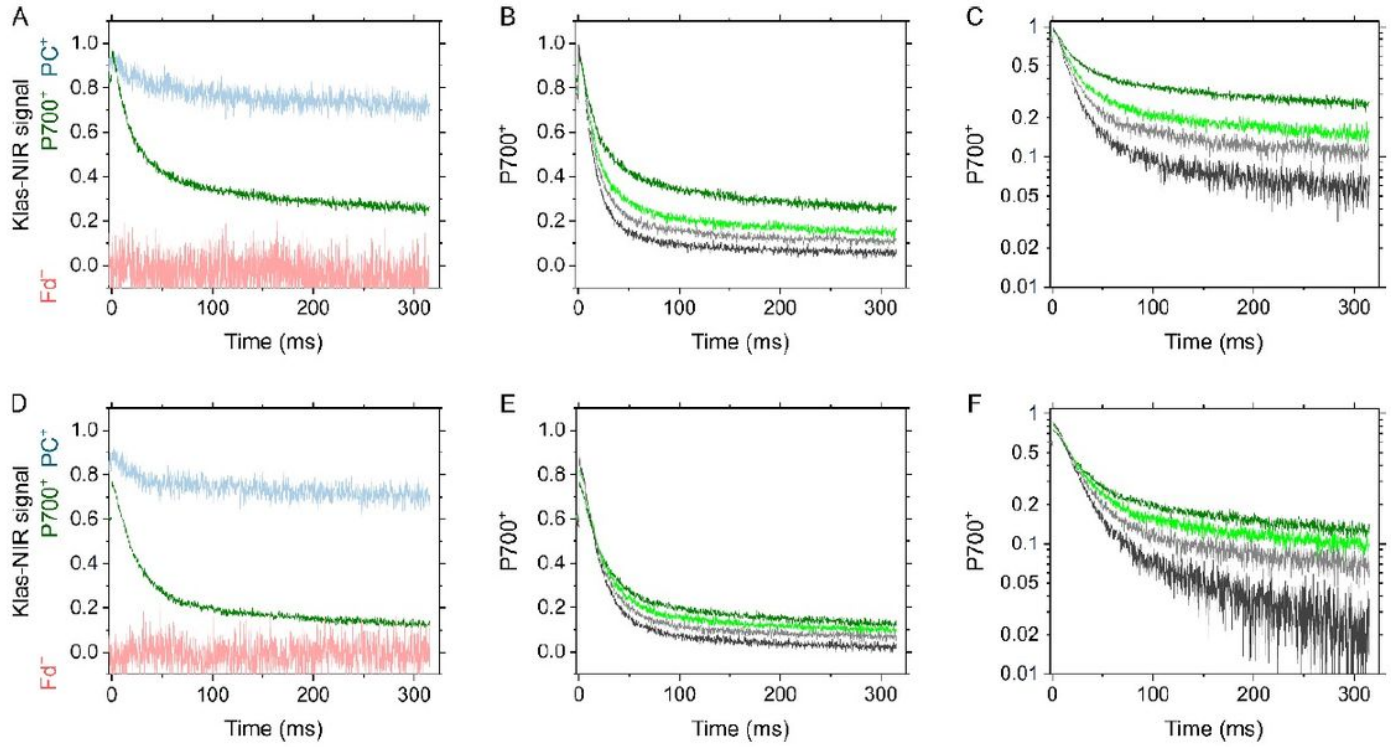

Figure 10

Effects of a short-saturation flash on the redox state around PSI in the C3 plant mustard (A–C) and the C4 plant maize (D–F). (A, D) Reduction kinetics of P700+ (green) in response to a 5 µs-short saturation flash after far-red light illumination for 10 s. Far-red light was provided at the maximum intensity (20, the value defined by the Walz software). Deconvoluted signals to plastocyanin (PC+, blue) and ferredoxin (Fd−, red) are also shown. All the Klas-NIR signals were normalized within the range from the minimum 0 to the maximum 1. The maximum reduction/oxidation levels of each component were determined as shown in Supplemental Fig. S2. The signal to Fd− has negative values. (B, E) Reduction kinetics of P700+ by a short saturation flash at different lengths (5, green; 10, light green; 20, light grey; and 50 µs, grey respectively) after far-red light illumination for 10 s. The kinetics are also shown with the logarithmic scale at y-axis (C, F). The representative traces of independent experiments (n = 3, biological replicates) are shown.

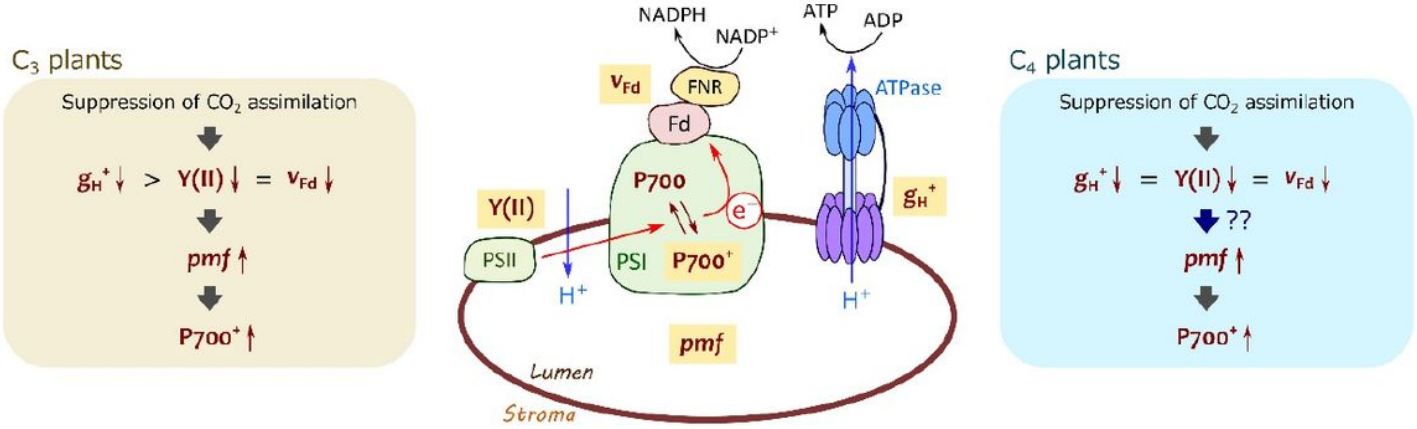

Figure 11

A brief illustration of mechanism for P700 oxidation in C3 and C4 plants. In C3 plants, proton conductance of chloroplast ATP synthase (gH+) decreases with the suppression of photosynthetic CO2 assimilation greater than photosynthetic linear electron flow reflected in effective quantum yield of PSII, Y(II), and ferredoxin (Fd−) oxidation rate (vFd), resulting in the increase in proton motive force (pmf) to induce P700 oxidation. In C4 plants, pmf increases with the suppression of photosynthetic CO2 assimilation, although gH+ decreases concomitantly with Y(II) and vFd.

Supplementary Files

This is a list of supplementary files associated with this preprint. Click to download.

- SupplementsC4KlasNir20210205.pdf